

# Bulge $n$ and $B/T$ in High Mass Galaxies: Constraints on the Origin of Bulges in Hierarchical Models

Tim Weinzirl<sup>1</sup>, Shardha Jogee<sup>1</sup>, Sadegh Khochfar<sup>2,3</sup>, Andreas Burkert<sup>4</sup>, John Kormendy<sup>1</sup>

## ABSTRACT

The properties of galaxy components provide key constraints for models of galaxy evolution. With an iterative 2D decomposition technique based on GALFIT, we perform bulge-disk and bulge-disk-bar decomposition on  $H$ -band images of a complete sample of 146 bright ( $M_B < -19.3$ ) moderately inclined ( $i \leq 70^\circ$ ) spirals from the OSU Bright Spiral Galaxy Survey. The sample has primarily spirals with Hubble type S0/a to Sc and high stellar mass ( $M_\star \geq 1.0 \times 10^{10} M_\odot$ ). Our results are: (1) From bulge-disk-bar decomposition, we find an  $H$ -band bar fraction of  $\sim 58\%$  (85/146), which is in excellent agreement with the published bar fraction of 60% based on ellipse fits. (2) We estimate that 70% of the stellar mass is in disks, 10% is in stellar bars and 20% is in bulges (with  $\sim 15\%$  in  $n > 2$  bulges and  $\sim 5\%$  in  $n \leq 2$  bulges). (3) *A strikingly large fraction ( $\sim 60\%$ ) of bright spirals have low  $n \leq 2$  bulges: such bulges exist in barred and unbarred galaxies across all Hubble types, and their  $B/T$  ranges from 0.01 to 0.4, with most having  $B/T \leq 0.2$ .* Only a small fraction ( $\sim 5\%$ ) of bright spirals have high  $n \geq 4$  bulges and these have primarily large  $B/T > 0.2$ . The remaining fraction ( $\sim 35\%$ ) of bright spirals have intermediate  $2 < n < 4$  bulges with a mean  $B/T$  of 0.23. (4) About 64% (68%) of high mass spirals with  $n \leq 2$  ( $B/T \leq 0.2$ ) bulges host bars. This suggests that spontaneous and tidally-induced bars may play a part in forming a large fraction of such bulges. (5) We compare the observed bulge  $B/T$  and  $n$  in high mass spirals with predictions from a set  $\Lambda$ CDM cosmological semi-analytical models. In the models, a bulge with  $B/T \leq 0.2$  can exist in a galaxy with a past major merger, only if the last major merger occurred at  $z > 2$  (lookback time  $> 10$  Gyr), and the fraction ( $\sim 3\%$ ) of high mass spirals which have undergone a past major merger and host a present-day bulge with  $B/T \leq 0.2$  is *a factor of over fifteen smaller* than the observed fraction ( $\sim 66\%$ ) of high mass spirals with  $B/T \leq 0.2$ . Thus, *bulges built via major mergers seriously fail to account for most of the low  $B/T \leq 0.2$  bulges present in over 60% of high mass spirals.* The majority of low  $B/T \leq 0.2$  bulges in high mass galaxies exist in systems that have experienced only minor mergers, and no major mergers. These bulges can be built via minor mergers and secular processes. We explore one realization of the model focusing on bulges built via satellite stars in minor mergers and find good agreement with the observations. Future models will explore secular processes.

*Subject headings:* galaxies: bulges — galaxies: evolution — galaxies: formation — galaxies: fundamental parameters — galaxies: interactions — galaxies: structure

<sup>1</sup>Department of Astronomy, University of Texas at Austin, Austin, TX

<sup>2</sup>Sub-Department of Astrophysics, University of Oxford, Denys Wilkinson Bldg., Keble Road, OX1 3RH, Oxford, UK

<sup>3</sup>Max Planck Institut für extraterrestrische Physik, P.O Box 1312, D-85478 Garching, Germany

<sup>4</sup> Universitäts-Sternwarte München, Scheinerstr. 1, 81679 München, Germany

## 1. Introduction

The formation of galaxies is a classic problem in astrophysics. Contemporary galaxy formation models combine the well-established  $\Lambda$  Cold Dark Matter ( $\Lambda$ CDM) cosmology, which describes behavior of dark matter on very large scales, with baryonic physics to model galaxy formation. In the early Universe, pockets of dark matter decoupled from the Hubble flow, collapsed into virialized halos, and then clustered hierarchically into larger structures. Meanwhile, gas aggregated in the interiors of the halos to form rotating disks, which are the building blocks of galaxies (Steinmetz & Navarro 2002; Cole et al. 2000). Such disks are typically destroyed during major mergers of galaxies with mass ratio  $M_1/M_2 > 1/4$  (e.g. Steinmetz & Navarro 2002; Naab & Burkert 2003; Burkert & Naab 2004; Mihos & Hernquist 1996). When the mass ratio is close to unity, the remnant is a spheroid with properties close to that of a classical bulge, namely a steep de Vaucouleurs  $r^{1/4}$  surface brightness profile and a high ratio of random-to-ordered motion ( $V/\sigma$ ). We shall return to this point in § 5. Within this hierarchical framework, the disk of spiral galaxies forms when gas of higher specific angular momentum subsequently accretes around the bulge (Steinmetz & Navarro 2002; Burkert & Naab 2004).

$\Lambda$ CDM-based simulations of galaxy formation face several challenges. One issue is the angular momentum problem; simulated galaxy disks have smaller scalelengths and, therefore, less specific angular momentum than their counterparts in nature (Navarro & Steinmetz 2000; Burkert & D’Onghia 2004; D’Onghia et al. 2006). A second issue is the problem of bulgeless or low bulge-to-total mass ratio ( $B/T$ ) spirals. Within the  $\Lambda$ CDM paradigm, galaxies that had a past major merger at a time when its mass was a fairly large fraction of its present-day mass are expected to have a significant bulge with large  $B/T$  and high Sérsic index. Depending on the merger history and hence the fraction of spiral galaxies that fulfill this criterion (see § 5.8) we can end up with a small or large fraction of present-day galaxies with low  $B/T$ . There is rising evidence that low  $B/T$  and bulgeless galaxies are quite common in the local Universe. Locally, late-type Sd galaxies often harbor no bulge (Böker et al. 2002; Kormendy & Kennicutt 2004). Kautsch et al. (2006), as well as Barazza, Jogee & Marinova (2007; 2008) find from the analysis of several thousand late-type SDSS galaxies that 15-20% of such disk galaxies out to  $z \sim 0.03$  appear bulgeless. Of the 19 local galaxies ( $D < 8$  Mpc) with  $V_c > 150$   $\text{km s}^{-1}$ , 11 (58%) have pseudobulges instead of merger-built classical bulges (Kormendy 2008).

The emerging statistics on the fraction of bulgeless ( $B/T \sim 0$ ) galaxies in low mass spirals from the above studies (Kautsch et al. 2006; Barazza, Jogee & Marinova 2008; Kormendy 2008), provide important first constraints. Theoretical work by Koda et al. (2007) conclude the survival of disk-dominated systems in a  $\Lambda$ CDM universe is compatible with observational constraints provided classical bulges form only in mergers where  $M_1/M_2 > 0.3$  and the primary halo has virial velocity  $V_{vir} > 55$   $\text{km s}^{-1}$ . However, many questions still remain unanswered. What is the distribution of  $B/T$  ratios along the Hubble sequence, in both high mass and low mass galaxies? How does this distribution compare to predictions from hierarchical models of galaxy evolution? To the best of our knowledge, a quantitative comparison between the observed distributions of bulge  $B/T$  and  $n$ , and the predictions from  $\Lambda$ CDM-based simulations of galaxy evolution has not been attempted. In fact, it remains unclear how serious the problem of low  $B/T$  galaxies is. This study is an attempt to derive robust observational constraints on bulge properties and to attempt such a comparison with models.

Completely resolving the issue of low  $B/T$  systems will require understanding the different types of bulges and their formation pathways. Bulges are commonly divided in several groups: classical bulges, boxy/peanut bulges, and ‘pseudobulges’ or disk bulges. Classical bulges are believed to be built by major

mergers ( $M_1/M_2 \geq 1/4$ ) and the associated violent relaxation of stars. They are associated with modest-to-high bulge Sérsic indices, in the range  $2 < n < 6$  (Hopkins et al. 2008, in prep.; Springel et al. 2005; Robertson et al. 2006; § 5.8). Boxy/peanut bulges are believed to be the result of vertical resonances and buckling instabilities in bars, which are viewed at high inclination (Combes & Sanders 1981; Combes et al. 1990; Pfenniger & Norman 1990; Bureau & Athanassoula 2005; Athanassoula 2005; Martinez-Valpuesta et al. 2006). Pseudobulges or disk bulges are believed to form as a result of gas inflow into the central kiloparsec and subsequent star formation building a compact disk, high  $v/\sigma$  stellar component (Kormendy 1993; Jogee 1999; Kormendy & Kennicutt 2004, hereafter KK04; Jogee, Scoville, & Kenney 2005; Athanassoula 2005; Kormendy & Fisher 2005). Pseudobulges tend to have a bulge  $n < 2.5$  (Kormendy & Fisher 2005; Fisher & Drory 2008).

One possibility for the formation of disk bulges or pseudobulges is the idea of secular evolution (Kormendy 1993; KK04; Jogee, Scoville, & Kenney 2005), where a stellar bar or globally oval structure in a *non-interacting* galaxy drives the gas inflow into the inner kpc via shocks and gravitational torque. Another idea for building disk bulges is that the gas inflow into the inner kiloparsec is driven by *external non-secular processes*, such as tidal interaction and minor mergers. The gas inflow in such cases can be caused by a tidally induced bar (e.g., Quinn et al. 1993; Hernquist & Mihos 1995), and by tidal torques from the companion. The subsequent central star formation can still form a compact high  $v/\sigma$  stellar component, *aka* pseudobulge.

Throughout this paper, we avoid making any *a priori* assumptions about the origin of different types of bulges by simply referring to them according to their bulge Sérsic index  $n$  or bulge-to-total mass ratio ( $B/T$ ). We consider bulges of high ( $n \geq 4$ ), intermediate ( $2 < n < 4$ ) and low ( $n \leq 2$ ) index, as well as those of low or high  $B/T$ .

The structural properties of galaxy components, such as bulges, disks, and bars can be derived through the decomposition of the 2D light distribution, taking into account the PSF. Many early studies have performed only two component 2D bulge-disk decomposition (e.g., Allen et al. 2006; Byun & Freeman 1995; de Jong 1996; Simard 1998; Wadadekar et al. 1999), ignoring the contribution of the bar, even in strongly barred galaxies. However, recent work has shown that it is important to include the bar in 2D decomposition of barred galaxies, else the  $B/T$  ratio can be artificially inflated, and bulge properties skewed (e.g., Laurikainen et al. 2005, 2007). Furthermore, since most ( $\geq 60\%$ ) bright spiral galaxies are barred in the NIR (Eskridge et al. 2000; Laurikainen et al. 2004; Marinova & Jogee 2007, hereafter MJ07; Menendez-Delmestre et al. 2007), the inclusion of the bar is quite important. This has led to several recent studies, where 2D bulge-disk-bar decomposition are being performed (e.g. Laurikainen et al. 2007; Reese et al. 2007; Gadotti & Kauffmann 2007).

Another advantage of bulge-disk-bar decomposition over bulge-disk decomposition is that the former allows us to constrain the properties of the bar itself. Bars provide the most important internal mechanism for redistributing angular momentum in baryonic and dark matter components (e.g. Weinberg 1985; Debattista & Sellwood 1998, 2000; Athanassoula 2002; Berentzen, Shlosman, & Jogee 2006). They efficiently drive gas inflows into the central kpc, feed central starbursts (Elmegreen 1994; Knapen et al. 1995; Hunt & Malakan 1999; Jogee et al. 1999; Jogee, Scoville, & Kenney 2005; Jogee 2006) and lead to the formation of disk or pseudobulges (see above). Furthermore, the prominence of strong bars out to  $z \sim 1$  over the last 8 Gyr (Jogee et al. 2004; Sheth et al. 2008) suggest that bars have been present over cosmological times and can shape the dynamical and secular evolution of disks. Thus, quantifying bar properties, such as the fractional light and mass ratio (Bar/ $T$ ), can yield insight into these processes.

In this paper, we constrain the properties of bulges and bars along the Hubble sequence, and compare our results to  $\Lambda$ CDM-based simulations of galaxy evolution. In § 2, we define our complete sample of  $\sim 146$  bright ( $M_B < -19.3$ ) moderately inclined ( $i \leq 70^\circ$ ) spirals from the Ohio State University Bright Spiral Galaxy Survey (OSUBSGS; Eskridge et al. 2002), which is widely used as the local reference sample for bright spirals by numerous studies (e.g., Eskridge et al. 2000; Block et al. 2002; Buta et al. 2005; MJ07 ; Laurikainen et al. 2004, 2007). In § 3, we perform 2D bulge-disk and bulge-disk-bar decompositions of  $H$ -band images using GALFIT (Peng et al. 2002), and derive fractional light ratios ( $B/T$ , Bar/ $T$ , Disk/ $T$ ), as well as Sérsic indices and half light radii or scale lengths. Tests to verify the robustness of our decompositions are presented in § 4. In § 5, we present our results. Specifically, the total stellar mass present in bulges, disks, and bars is calculated § 5.2. In § 5.3, the distribution of bulge Sérsic index  $n$  and  $B/T$  as a function of galaxy Hubble type and stellar mass is presented, and the surprising prevalence of bulges with low Sérsic index  $n$  and low  $B/T$  established. A comparison with other works is presented in § 5.4. We examine how Bar/ $T$  and bar fraction change as a function of host galaxy properties in § 5.5. In § 5.8, we compare our observed distribution of bulge  $B/T$  and  $n$  in high mass ( $M_\star \geq 1.0 \times 10^{10} M_\odot$ ) spirals with predictions from  $\Lambda$ CDM cosmological semi-analytical models. § 6 summarizes our results.

## 2. Sample Properties

### 2.1. OSUBSGS

Our dataset is derived from the 182  $H$ -band images from the public data release of the Ohio State University Bright Spiral Galaxy Survey (OSUBSGS; Eskridge et al. 2002). These galaxies are a subset of the RC3 catalog that have  $m_B \leq 12$ , Hubble types  $0 \leq T \leq 9$  (S0/a to Sm) ,  $D_{25} \leq 6'.5$ , and  $-80^\circ < \delta < +50^\circ$ . Imaging of OSUBSGS galaxies spans optical and near infrared (NIR) wavelengths with  $BVRJHK$  images available for most galaxies. We choose to use the NIR images rather than optical ones for several reasons. Firstly, NIR images are better tracers of the stellar mass than optical images, and the mass-to-light ratio is less affected by age gradients or dust gradient. Secondly, obscuration by dust and SF are minimized in the NIR, compared to the optical. As the  $K$ -band images are of poor quality, we settle on using the  $H$ -band images.

The OSUBSGS is widely used as the local reference sample for bright spirals by numerous studies (e.g. Eskridge et al. 2000; Block et al. 2002; Buta et al. 2005; MJ07 ; Laurikainen et al. 2004, 2007). Thus, there are numerous complementary results that we can use or compare to. In particular, MJ07 have identified bars in this sample using quantitative criteria based on ellipse fitting, and characterized their sizes, position angles, and ellipticities.

OSUBSGS is a magnitude-limited survey with objects whose distances range up to  $\sim 60$  Mpc. Faint galaxies are inevitably missed at larger distances, resulting in the absolute magnitude distribution in Figure 1. We compare the  $B$ -band LF of this sample with a Schechter (Schechter 1976) LF (SLF) with  $\Phi^* = 5.488 \times 10^{-3} \text{ Mpc}^{-3}$ ,  $\alpha = -1.07$ , and  $M_B^* = -20.5$  (Efstathiou, Ellis & Peterson 1988) in Figure 2. The volume used to determine the number density in each magnitude bin is

$$V_{max} = \frac{4\pi}{3} d_{max}^3(M), \quad (1)$$

where

$$d_{max}(M) = 10^{1+0.2(m_c-M)} \quad (2)$$

is the maximum distance out to which a galaxy of absolute magnitude  $M$  can be observed given the cutoff magnitude  $m_c$ . If the SLF is representative of the true LF, then Figure 2 suggests that the OSUBSGS sample starts to be seriously incomplete at  $M_B > -19.3$ , while at the brighter end (-19.3 to -23) the shape of its LF matches fairly well the SLF. We thus conclude that the sample is reasonably complete for bright ( $M_B < -19.3$  or  $L_B > 0.33 L^*$ ) galaxies.

We exclude highly inclined ( $i > 70^\circ$ ) galaxies for which structural decomposition does not yield accurate results. Thus, our final sample S1 consists of 146 bright ( $M_B < -19.3$ ) moderately inclined ( $i \leq 70^\circ$ ) spirals with Hubble types mainly in the range S0/a to Sc (Figure 1). Of the 127 for which we could derive stellar masses (see § 2.2, most have stellar masses  $M_\star \geq 1.0 \times 10^{10} M_\odot$  (Figure 3). Table 1 summarizes the morphologies, luminosities, and stellar masses of the sample. Note that there are few galaxies of late Hubble types (Scd or later) and we do not draw any conclusions on such systems from our study. In a future paper, we will tackle galaxies of lower mass and later Hubble types.

## 2.2. Stellar Masses

We derive global stellar masses for most of the OSUBSGS sample galaxies using the relation between stellar mass and rest-frame  $B - V$  color from Bell et al. (2003). Using population synthesis models, the latter study calculates stellar  $M/L$  ratio as a function of color using functions of the form  $\log_{10}(M/L) = a_\lambda + b_\lambda \times \text{Color} + C$ , where  $a_\lambda$  and  $b_\lambda$  are bandpass dependent constants and  $C$  is a constant that depends on the stellar initial mass function (IMF). For the  $V$  band Bell et al. (2003) find  $a_\lambda = -0.628$  and  $b_\lambda = 1.305$ ; assuming a Kroupa (1993) IMF, they find  $C = -0.10$ . This yields an expression for the stellar mass in  $M_\odot$  for a given  $B - V$  color:

$$M_\star = v_{lum} 10^{-0.628+1.305(B-V)-0.10}, \quad (3)$$

where

$$v_{lum} = 10^{-0.4(V-4.82)}. \quad (4)$$

Here,  $V_{lum}$  is the luminosity parametrized in terms of absolute  $V$  magnitude.

How reliable are stellar masses determined from this procedure? Clearly, the above relationship between  $M_\star$  and  $B - V$  cannot apply to all galaxies, and must depend on the assumed stellar IMF, and range of ages, dust, and metallicity. However, it is encouraging to note that several studies (Bell et al. 2003; Drory et al. 2004) find generally good agreement between masses based on broad-band colors and those from spectroscopic (e.g. Kauffmann et al. 2003) and dynamical (Drory et al. 2004) techniques. Typical errors are within a factor of 2 to 3.

We used this relation to compute stellar masses for 127 (87%) objects. The remainder did not have  $B - V$  colors available in the Hyperleda database or RC3. The mass distribution is summarized in Figure 3. Individual masses are listed in Table 1. This sample of 127 galaxies is referenced henceforth as sample S2.

## 3. Method and Analysis

The structural properties of galaxy components, such as bulges, disks, and bars can be derived through the decomposition of the 2D light distribution, taking into account the PSF. There are several softwares

for 2D luminosity decomposition, including GIM2D (Simard et al. 2002), GALFIT (Peng et al. 2002), and BUDDA (de Souza et al. 2004). The latter two allow bulge-disk-bar decomposition, while the former only allows bulge-disk decomposition

Most previous work has addressed 2D bulge-disk decomposition only. Allen et al. (2006), for example, performed bulge-disk decomposition of  $B$ -band images with GIM2D on 10,095 galaxies from the Millennium Galaxy Catalog (Liske et al. 2003; Driver et al. 2005). However, recent work (e.g., Laurikainen et al. 2005; Graham & Balcells, in preparation) has shown that the  $B/T$  ratio can be artificially inflated in a barred galaxy unless the bar component is included in the 2D decomposition. The fact that most ( $\geq 60\%$ ) bright spiral galaxies are barred in the NIR (Eskridge et al. 2000; Laurikainen et al. 2004; MJ07; Menendez-Delmestre et al. 2007), further warrants the inclusion of the bar. Another advantage of bulge-disk-bar decomposition is that it allows us to constrain the properties of the bar itself, and to constrain scenarios of bar-driven evolution (see § 1).

Motivated by these considerations, several studies have tackled the problem of 2D bulge-disk-bar decomposition. Laurikainen et al. (2005, 2007) have developed a 2D multicomponent decomposition code designed to model bulges, disks, primary and secondary bars, and lenses; they apply Sérsic functions to bulges and use either Sérsic or Ferrers functions to describe bars and lenses. Reese et al. (2007) have written a non-parametric algorithm to model bars in  $\sim 70$   $I$ -band images. Gadotti & Kauffmann (2007) are performing 2D bulge-disk-bar and bulge-disk decomposition of 1000 barred and unbarred galaxies from SDSS with the BUDDA software.

In this study, we perform 2D two-component bulge-disk decomposition and three-component bulge-disk-bar decomposition of the OSUBSGS sample with GALFIT. We note that Laurikainen et al. (2007) have also performed bulge-disk-bar decomposition on the OSUBSGS sample. However, there are also important complementary differences between our study and theirs. The technique softwares, and tests on the robustness performed in our study are different (see § 3 and § 4). Furthermore, unlike Laurikainen et al. (2007), we also compare the bulge-to-total ratio ( $B/T$ ) to predictions from hierarchical models of galaxy evolution (§ 5), and also present the distribution of bar-to-total ratio ( $\text{Bar}/T$ ).

### 3.1. Image Preparation

Running GALFIT on an image requires initial preparation. The desired fitting region and sky background must be known, and the PSF image, bad pixel mask (if needed), and pixel noise map must be generated. We addressed these issues as follows: (1) The GALFIT fitting region must be large enough to include the outer galaxy disk, as well as some sky region. Since cutting out empty regions of sky can drastically reduce GALFIT run-time, a balance was sought between including the entire galaxy and some decent sky region, while excluding large extraneous blank sky areas. (2) It is possible for GALFIT fit the sky background, but this is not recommended. When the sky is a free parameter, the wings of the bulge Sérsic profile can become inappropriately extended, resulting in a Sérsic index that is too high. Sky backgrounds were measured separately and designated as fixed parameters; (3) GALFIT requires a PSF image to correct for seeing effects. Statistics of many stars in each frame can be used to determine an average PSF. However, many of our images contain only a few stars. Instead, a high S/N star from each frame was used as a PSF; (4) We used ordered lists of pixel coordinates to make bad pixel masks, which are useful for blocking out bright stars and other image artifacts; (5) We had GALFIT internally calculate pixel noise maps for an image from the noise associated with each pixel. Noise values are determined from image header information

concerning gain, read noise, exposure time, and the number of combined exposures.

### 3.2. Decomposition Steps

Figure 4 summarizes our method of decomposition, which we now detail. GALFIT requires initial guesses for each component it fits. It uses a Levenberg-Marquardt downhill-gradient algorithm to determine the minimum  $\chi^2$  based on the input guesses. GALFIT continues iterating until the  $\chi^2$  changes by less than 5e-04 for five iterations (Peng et al. 2002). We recognize that a drawback to any least-squares method is that a local minimum, rather than a global minimum, in  $\chi^2$  space may be converged upon. We explore this possibility with multiple tests described in §4. We adopted an iterative process, involving three separate invocations of GALFIT, to perform 1-component, 2-component, and 3-component decomposition:

1. Stage 1 (single Sérsic): In Stage 1, a single Sérsic component is fitted to the galaxy. This serves the purpose of measuring the total luminosity, which is conserved in later Stages, and the centroid of the galaxy, which is invariant in later fits.
2. Stage 2 (exponential plus Sérsic): In Stage 2, the image is fit with the sum of an exponential disk and a Sérsic component. During the Stage 2 fit, the disk  $b/a$  and  $PA$  are held constant at values, which we take from the published ellipse fits of MJ07, as well as ellipse fits of our own. This procedure reduces the number of free parameters in the fit by fixing the disk  $b/a$  and  $PA$ , which are easily measurable parameters. It also prevents GALFIT from confusing the disk and bar, and artificially stretching the disk along the bar  $PA$  in an attempt to mimic the bar. As initial guesses for the Sérsic component in Stage 2, the output of Stage 1 is used. The Sérsic component in Stage 2 usually represents the bulge, in which case Stage 2 corresponds to a standard bulge-disk decomposition

However, in a few rare cases, where the galaxy only has a bar and a disk, the Sérsic component in Stage 2 represents a bar. The latter is recognizable by a low Sérsic index and large half-light radius.

3. Stage 3 (exponential plus two Sérsic components): In Stage 3, a three-component model consisting of an exponential disk, a Sérsic bulge, and a Sérsic bar is fit. As suggested by Peng et al. (2002), the bar can be well described by an elongated, low-index Sérsic ( $n < 1$ ) profile. As in Stage 2, the disk  $b/a$  and  $PA$  are held constant at values predetermined from ellipse fits. We provide initial guesses for the bar  $b/a$  and  $PA$ , based on ellipse fits of the images from MJ07 or analysis of the images in DS9. We provide GALFIT with input guesses for the bulge parameters, based on the output from Stage 2. In principle, it is also possible to generate reasonable guess parameters for the bulge and disk from a bulge-disk decomposition on a 1D profile taken along a select  $PA$ . As described in § 4.3, we also experiment with initial guesses derived in this way, and find that the final convergence solution is the same. We also note that GALFIT fixes the bulge  $b/a$  and does not allow it to vary with radius, while real bulges may have a varying  $b/a$ . We tested the impact of fixed and varying bulge  $b/a$  on the derived  $B/T$  (§ 4.1) and find that there is no significant change in  $B/T$ .

For objects with an AGN or a compact nuclear cluster, the bulge Sérsic index in the Stage 2 and Stage 3 models could grow excessively high, reaching values up to 20. We attended to this problem by fitting a PSF as a fourth component to all 49 objects whose initial fits had bulge Sérsic indices  $> 5$ . Twenty-eight of these objects are classified as AGN, based on the catalogs of Ho et al. (1997), Véron Catalog of Quasars & AGN, 12th Edition (Véron-Cetty & Véron 2006), and NED. Six extra objects are known to not be AGN

but are identified by Ho et al. (1997) as having HII nuclei. The remaining 15 objects do not have published nuclear line ratios to indicate if they host AGN. However, all appear to have bright compact nuclear sources, which could be nuclear star clusters or AGN. The fractional luminosities of the PSF components ( $PSF/T$ ) are typically a few percent or less, with several being  $< 1\%$ . A few are between 5-7%, and these are all confirmed AGN. The PSF luminosity was added back to the bulge in calculating  $B/T$ . Since  $PSF/T$  is generally small, this step introduces only a small change in the final  $B/T$  of the relevant galaxies.

GALFIT also allows a diskiness/boxiness parameter to be added to any Sérsic and exponential profile. We did not use this parameter for any bulge or disk profiles. Bars in general have boxy isophotes, and we could have included the diskiness/boxiness parameters in the bar profiles. However, it was found that adding boxiness to the bar profile did not change the model parameters significantly, even though the appearance of the residual images improved in some cases due to the change in bar shape. Accounting does not alter fractional luminosity, effective radius and scalelength, or Sérsic index by more than a small percentage. Consequently, we chose to neglect bar boxiness altogether.

### 3.3. Choosing the Best Fit Between Stage 2 and Stage 3

All objects in our sample were subjected to Stages 1, 2, and 3. Depending on whether a galaxy with a bulge is unbarred or barred, its best fit should be taken from the Stage 2 bulge-disk decomposition or the Stage 3 bulge-disk-bar decomposition, respectively. For objects with prominent bars, it is obvious that the Stage 3 model provides the best fit. However, it is more difficult to decide between Stage 2 versus Stage 3 fits in galaxies which host weak bars with no strong visual signature. In practice, we therefore applied the set of criteria below to each galaxy in order to select between the Stage 2 bulge-disk decomposition and Stage 3 bulge-disk-bar decomposition. Table 1 lists the model chosen for each galaxy.

For completeness, we note that for the few rare galaxies (see § 3.2), that only have a bar and a disk, the choice of a final solution is between the Stage 2 bar-disk decomposition and Stage 3 bulge-disk-bar decomposition. The same criteria below can be used to identify the best model.

1. GALFIT calculates a  $\chi^2$  and  $\chi^2_\nu$  for each model. It was found that  $\chi^2$  almost universally declines between the Stage 2 and Stage 3 fits for a given object. This is because in the Stage 3 fit, five extra free parameters (bar luminosity,  $r_e$ , Sérsic index,  $b/a$ , and  $PA$ ) are added with the Sérsic bar component, allowing GALFIT to almost always make a lower  $\chi^2$  model during Stage 3. However, this does not necessarily mean that the solution in Stage 3 is more correct physically. Thus, an increasing  $\chi^2$  was interpreted as a sign that the Stage 3 fit should not be adopted, but a decreasing  $\chi^2$  was not considered as a sufficient condition to adopt Stage 3.
2. In cases with prominent bars, a symmetric light distribution due to unsubtracted bar light was often found in the Stage 1 and Stage 2 bulge-disk residuals. This was strong evidence that the Stage 3 bulge-disk-bar fit be selected. NGC 4643 is shown in Figure 5 because it has a particularly striking bar residual; the corresponding fit parameters appear in Table 2. Note that in all figures and tables, we adopt the convention that  $PA$  values are positive/negative if they are measured from North counterclockwise/clockwise.
3. The Stage 2 and Stage 3 models were only selected so long as the model parameters were all well behaved. In unbarred galaxies, the Stage 3 model parameters might be unphysically large or small, in which case the Stage 2 fit was favored. Conversely, in galaxies with prominent bars, the bulge

component of the Stage 2 bulge-disk fit tends to grow too extended in size. Addition of a bar in the Stage 3 bulge-disk-bar fit removes this artifact, giving a more physical solution. An extreme example of this situation is the barred galaxy NGC 4548, which has a prominent bar and a faint disk. The Stage 2 fit, based on a Sérsic bulge and exponential disk, is highly inadequate to describe the bulge, disk, *and* the bar. It leads to an extremely extended bulge. The Stage 3 bulge-disk-bar fit, however, yields a believable fit with a prominent bar. The results of Stage 1, Stage 2, and Stage 3 are displayed in Figure 6 and Table 3.

4. Not all barred galaxies had unphysical Stage 2 models. Instead, the bulge could be stretched along the *PA* of the bar, giving the bulge a lower Sérsic index and larger effective radius. A Stage 3 model that returned the bulge to a size and shape more representative of the input image was favored over the Stage 2 fit. Figure 7 and Table 4 demonstrate this behavior in NGC 4902. We distinguish this effect from cases like NGC 4548 (Figure 6 and Table 3) where the Stage 2 fit is completely wrong.
5. In cases where there was no bar, GALFIT can sometimes be enticed into fitting a bar to any existing spiral arms, rings, or the clumpy disks of late-type spirals. Stage 3 fits in these cases could be discarded by noting the resulting discrepancies in appearance between the galaxy images and the Stage 3 model images. Examples of false bars are shown in Figure 8.
6. After fitting the whole sample and picking the best fit from either the Stage 2 bulge-disk decomposition or the Stage 3 bulge-disk-bar decomposition, we also performed the following extra tests. For our sample S1 of 146 bright ( $M_B < -19.3$ ) moderately inclined ( $i \leq 70^\circ$ ) spirals in the OSUBSGS survey, we determine the fraction (77/146 or  $\sim 53\%$ ) of spiral galaxies where a bulge-disk-bar decomposition was picked as the best fit for the *H*-band image. There are also eight galaxies with pure bar-disk fits. The *H*-band bar fraction, which is defined as the fraction of disk galaxies that are barred, is therefore  $58.2 \pm 4.08\%$  (85/146). We then compared our results ( $58.2\% \pm 4.08\%$ ) to the *H*-band bar fraction (60%) determined from ellipse fits of the OSUBSGS sample by MJ07, with a slightly more conservative inclination cut ( $i \leq 60^\circ$ ). The two numbers are in excellent agreement. As a further check to our fits, we compare the bar and unbarred classification for individual galaxies from our fits to those from MJ07, which were based on ellipse fits. Of the 74 galaxies, which we classify as barred and which are mutually fitted by MJ07, 55 (74.3%) are also classified as barred by MJ07. The remaining 19 (25.7%) galaxies are mainly weakly barred (with  $\text{Bar}/T$  below 0.08). Their RC3 optical types are weakly barred AB (10), barred B (7), and unbarred A (2).
7. In most previous bulge-disk and bulge-disk-bar 2D decomposition, the issue of parameter coupling and the systematic exploration of local versus global minima in  $\chi^2$  have been ignored. Quantifying how the parameters are coupled is important in measuring error bars for the model parameters. With 2D models containing several free parameters, this is not an easy task. We are currently investigating the calculation of error bars for two and three component GALFIT models from  $\chi^2$  surfaces. This is quite computationally expensive and requires a considerable time investment. We will explore these issues further in a future paper.

## 4. Extra Tests to Verify Correctness of Fits

### 4.1. Varying $b/a$ as a Function of Radius

Models generated with GALFIT do not allow the  $b/a$  of the bulge, disk, or bar to vary with radius. Since real bulges may have a varying  $b/a$ , it is legitimate to investigate what is the impact of fixing the bulge  $b/a$ , on the estimated  $B/T$ . We therefore performed the following test on NGC 4548. To mimic a model bulge of varying  $b/a$ , we fitted the bulge light of NGC 4548 with ten concentric Sérsic profiles of increasing  $r_e$  and varying  $b/a$ . The  $r_e$  of the outermost profile comes from the original bulge model (see Table 3) where  $b/a$  was kept constant with radius. The separation in  $r_e$  between adjacent profiles is 0.5 pixels (0.75"). The luminosity, Sérsic index,  $b/a$ , and  $PA$  of each profile were free parameters. The disk and bar components were fixed to the values in Table 3, as the emphasis was on the change in the bulge only.

Figure 9 compares the  $B/T$  obtained by fitting the bulge of NGC 4548 with a Sérsic model of constant  $b/a$  as opposed to a Sérsic model varying  $b/a$ . The bulge  $b/a$  (0.88),  $PA$  (-66.5), and  $B/T$  (13%) from the original Sérsic fit of constant  $b/a$  (Table 3) are indicated with horizontal lines on the 3 panels. The top two panels show the run of  $b/a$  (0.85 to 1.0) and  $PA$  (-90° to +90°) of the ten concentric Sérsic profiles. It can be seen that the Sérsic indices of the ten bulge models were generally higher toward the center and declined at larger  $r_e$ , indicating that the ‘fitted bulge is more concentrated at the center. The bottom panel shows the cumulative  $B/T$  calculated by summing all models with  $r \leq r_e$ : the last point representing the summed  $B/T$  from all ten components is 14.5%, in good agreement with the 13.0% value from the Sérsic fit of constant  $b/a$ . Thus, using Sérsic model of constant  $b/a$ , does not have any significant adverse impact on our derived  $B/T$  in NGC 4548.

### 4.2. Fitting Artificially Simulated Images

An elementary test is to determine if GALFIT can recover the known parameters of artificially simulated noisy images. The images were simulated by taking parametric model images produced by GALFIT, and adding noise to the images with the PyFITS module for Python (Barrett & Bridgman 1999). Noise in each pixel was calculated by adding in quadrature the noise due to the source, sky, and read noise. The standard deviation of pixel noise in electrons was computed as

$$\sigma = \sqrt{T_{\text{source}} + T_{\text{sky}} + T_{\text{read}}^2}, \quad (5)$$

where  $T_{\text{source}}$  is the number of electrons due to the source,  $T_{\text{sky}}$  is the number of electrons due to the sky, and  $T_{\text{read}}$  is number of electrons added due to detector read noise. The contribution due to detector dark current was very small and therefore neglected. The offset added to each pixel was drawn from a normal distribution centered at zero with standard deviation  $\sigma$ .

Our test sample consisted of six bulge-disk-bar and four bulge-disk models with two models of each group containing extra PSF components. Examples of the artificially simulated noise-added models are shown in Figure 10. These images were subjected to the 2D decomposition procedure outlined in Figure 4. GALFIT reproduced the known parameters quite closely. The mean surface brightness inside the disk scalelength spanned 4.5 magnitudes.  $B/T$  and  $D/T$  were recovered to within  $\pm 5\%$  in most cases. In a few cases, the deviation was as high as  $\pm 10\%$ .

In addition, for the models with PSFs, very high Sérsic indices were obtained in the Stage 2 and Stage 3 fits before extra PSF components were added to the models. The success of this test is evidence that

GALFIT is able to converge to the absolute minimum in  $\chi^2$  space for our bulge-disk and bulge-disk-bar decompositions when the input is the sum of parametric functions.

#### 4.3. Using 1D Decomposition To Generate Guesses for Bulge Parameters

It is important to verify that GALFIT converges to the same solution even if the initial guesses for the bulge parameters in Stage 2 and 3 are different. Bulge-disk decomposition from 1D profiles provides an alternative means of generating initial guesses. While 1D bulge-disk decompositions of radial profiles along the bar major axis can be influenced by the bar, decomposition of cuts along the bar minor axis will not be influenced as heavily. The resulting bulge and disk parameters should be adequate guesses for Stage 3 of our 2D decomposition method.

We tested the robustness of our Stage 3 fits by extracting initial guesses for the bulge and disk using 1D decomposition along the bar minor axis. The nonlinear least-squares algorithm designed to perform the 1D decomposition simultaneously fits the sky-subtracted profiles with the sum of a Sérsic bulge and an exponential disk, while ignoring the PSF. The results from the 1D decomposition include a bulge magnitude,  $r_e$ , Sérsic index, disk magnitude, and disk scalelength.

The robustness of several bulge-disk-bar fits were tested by using the results of the 1D decomposition as input to Stage 3. The 1D decompositions do not provide information about the axis ratio ( $b/a$ ) or  $PA$ , so these parameters for the bulge were estimated by eye; for the disk, the  $b/a$  and  $PA$  were fixed to the values determined by ellipse fitting, as described in §3.2. The initial bar parameters were unchanged from the earlier Stage 3 fits. In all cases, the new models were identical to the Stage 3 models. As an example, Table 5 compares Stage 3 input derived from 1D decomposition and GALFIT for NGC 4548 and NGC 4643. In each case, both sets of input reproduced the same results.

### 5. Results and Discussion

#### 5.1. Impact of Bars in 2D Decomposition

From the Stage 2 bulge-disk decomposition and Stage 3 bulge-disk-bar decompositions, which we performed on all objects (§ 3.2) we saw firsthand the effects of adding a bar to the fit of a barred galaxy. We summarize below some of these effects in order to underscore the importance of including a bar component in the 2D luminosity decomposition of barred galaxies

1. During the Stage 2 bulge-disk decomposition of a barred galaxy, the luminosity which comes from the galaxy’s disk, bulge, *and bar* gets distributed only between two model components: the model bulge and disk. Since the disk  $b/a$  and  $PA$  are measured independently and held constant during the fits, the Stage 2 model tends to distort the bulge in order to fit the bar. Thus, the bulge in the Stage 2 bulge-disk decomposition of a barred galaxy can be artificially long or too bright and extended. When a model bar component is added in the Stage 3 bulge-disk-bar decomposition of a barred galaxy, it forces a reshuffling of the luminosity between the three components. Generally, the bulge declines in luminosity, whereas light can be either taken from, or added back, to the disk.
2. We find that the inclusion of a bar component in the Stage 3 bulge-disk-bar decomposition of a barred galaxy reduces the bulge fractional luminosity  $B/T$ , compared to the Stage 2 bulge-disk decomposition.

For our 77 barred galaxies, the reductions correspond to factors of less than 2, 2 to 4, and above 4, in 34%, 28%, and 38% of barred galaxies, respectively. The larger changes in  $B/T$  occur in very strongly barred galaxies, where a prominent bar cause the Stage 2 bulge-disk decomposition to overestimate the bulge. For instance,  $B/T$  declines in both of NGC 4643 (Figure 5 and Table 2) and NGC 4548 (Figure 6 and Table 3). In the latter case,  $B/T$  is reduced by a factor of 5 between Stage 2 and Stage 3. These examples underscore the importance of including bars in 2D luminosity decomposition of very strongly barred galaxies.

3. The scalelength of the disk is generally unchanged by including the bar. NGC 4548 (Figure 6 and Table 3) is a good example. Sometimes, however, the disk from the Stage 2 bulge-disk decomposition of a barred galaxy is erroneous due to a poor fit. The disk parameters from the Stage 3 bulge-disk-bar decomposition are quite different in such cases. NGC 4643 (Figure 5 and Table 2) illustrates this behavior.

We find that for our sample S1 of 146 bright ( $M_B < -19.3$ ) moderately inclined ( $i \leq 70^\circ$ ) spirals (Figure 1) in the OSUBSGS survey, 77/146 or  $\sim 53\%$  are better fit with a Stage 3 bulge-disk-bar decomposition than a Stage 2 bulge-disk decomposition. There are also 8 galaxies with pure bar-disk fits. As stated in § 3.3, the resulting  $H$ -band bar fraction ( $58.2\% \pm 4.08\%$  or 85/146) is in excellent agreement with the  $H$ -band bar fraction of 60% reported by MJ07 based on ellipse fits of the OSUBSGS sample, with a slightly more conservative inclination cut ( $i \leq 60^\circ$ ). Furthermore, from a comparison of the bar and unbarred classification for individual galaxies from our fits to those based on ellipse fits from MJ07, we find the following. Of the 74 galaxies, which we classify as barred and which are mutually fitted by MJ07, 55 (74.3%) are also classified as barred by MJ07. The remaining 19 (25.7%) galaxies are mainly weakly barred (with  $Bar/T$  below 0.08). Their RC3 optical types are weakly barred AB (10), barred B (7), and unbarred A (2).

## 5.2. Mass in Bulges, Disks, and Bars

The fractional  $H$ -band luminosities in the bulge, disk, and bar ( $B/T$ ,  $D/T$ ,  $Bar/T$ ) of each galaxy can be considered as a fractional mass if we assume that the same mass-to-light ( $M/L$ ) ratio can be used to convert the  $H$ -band luminosities of both the numerator ( $B$ ,  $D$ , or Bar) and the denominator ( $T$ ) terms into a stellar mass. This is not an unreasonable assumption as the  $H$ -band  $M/L$  ratio is not very sensitive to differences in dust or age that might exist between the bulge, disk, and bar. The uncertainties in  $M/L$  can be estimated by looking at population synthesis models. Charlot, Worthey, & Bressan (1996) find that for idealized galaxies with a single generation of stars, the uncertainties in  $M/L$  ratio due to different input stellar models and spectra are roughly  $\pm 35\%$  for a fixed metallicity and IMF. Furthermore, as the age of a stellar population varies from  $\sim 0.5$  Gyr to 10 Gyr, the  $K$ -band  $M/L$  ratio rises by a factor of  $\sim 2$  to 3 (Charlot 1996). Asymptotic giant branch (AGB) stars dominate the NIR light for ages between 0.1 and 1 Gyr, while red giant branch (RGB) and supergiant branch (SGB) stars dominate between 1 Gyr and 10 Gyr.

In this paper, we convert the  $B/T$  light ratio determined from  $H$ -band images to a  $B/T$  mass ratio by assuming a constant mass-to-light ( $M/L$ ) in the  $H$ -band for both the bulge and the rest of the galaxy. Central regions of galaxies often harbor intense episodes of star formation. If the bulge is younger than the disk and happens to harbor star formation and a significant young population of massive stars, then our prescription could *overestimate* the true  $B/T$  mass ratio. This would make our current results on the high fraction of low  $B/T$  bulges even stronger.

On the other hand, if bulges are much older than the disks, then our prescription would underestimate the true  $B/T$  mass ratio. If we assume an extreme case where bulges are  $\sim 12$  Gyr and the disk light is dominated by a young 3 Gyr population, our assumption of a constant  $H$ -band  $M/L$  ratio would underestimate the true  $B/T$  by a factor of  $\leq 2$  (Charlot 1996). In several sections of the paper (e.g., § 5.3, § 5.8), we illustrate how our main results would change if the true  $B/T$  was higher by up to a factor of 2.

Using the total galaxy stellar mass from § 2.2, the fractional masses can be converted into absolute masses. (We do not convert the  $H$ -band luminosity directly into a mass as the  $H$ -band images do not have photometric calibration). The results are shown in Table 6. For our sample S1 of 146 bright ( $M_B < -19.3$ ) moderately inclined ( $i \leq 70^\circ$ ) spirals, we find that  $\sim 70\%$  of the stellar mass is in disks,  $\sim 10\%$  is in stellar bars and  $\sim 20\%$  is in bulges (with  $\sim 15\%$  in  $n > 2$  bulges and  $\sim 5\%$  in  $n \leq 2$  bulges). Thus while bulges with  $n \leq 2$  are highly ubiquitous (see next section), they only account for a small fraction of the total stellar mass budget.

Figure 11 shows the stellar mass for bulges, disks, and bars along the Hubble sequence.

It is useful to compare our results to those of Driver et al. (2006), who performed bulge-disk decomposition of  $B$ -band images with GIM2D on 10,095 galaxies from the Millennium Galaxy Catalog (Liske et al. 2003; Driver et al. 2005). They found 68.6% of the stellar mass to be in disks, and 32.6% in bulges (with 30.8% in high  $n$  bulges, and 1.8% in low  $n \leq 2$  bulges). Their study thus finds a higher stellar mass fraction in all bulges (32.6% vs our 20.2%), and in high  $n$  bulges (30.8% vs our 15.5%), and a lower fraction in low  $n \leq 2$  bulges (1.8% vs our 4.7%), and disks+bars (68.6% vs our 69.9% + 9.9%). This difference can be assigned to the fact that the Driver et al. (2006) study did not perform bulge-disk-bar fits and thus, their  $B/T$  ratios may be skewed to higher values.

### 5.3. Distribution of Bulge Index and $B/T$

Figure 12 shows the individual and mean  $B/T$  and bulge Sérsic index, plotted, as a function of Hubble type and galaxy stellar mass. Barred and unbarred galaxies are shown separately. Figure 13 shows the relationship between bulge index and  $B/T$ .

We first consider the  $B/T$  values in Figure 12. The mean  $B/T$  in barred galaxies is lower than in unbarred galaxies, but there is a large overlap in the individual values. The offset in the mean  $B/T$  of barred and unbarred galaxies reported here, agrees with the result of Laurikainen et al. (2007; see § 5.4) on the same sample. We also note that  $B/T$  does not correlate with Bar/T (Fig. 14): aside from the 6 galaxies with large Bar/T ( $> 0.3$ ), most galaxies have moderate Bar/T and a wide range of  $B/T$  is seen at each Bar/T. This is reassuring and suggests that the bar fit is not arbitrarily biasing the  $B/T$  values. The distribution of Bar/T is further discussed in § 5.5.

How does the  $B/T$  vary as a function of Hubble type and galaxy stellar mass? Bulges with very high  $B/T$  ( $> 0.4$ ) exist primarily in galaxies with high mass ( $M_\star > 6 \times 10^{10} M_\odot$ ) and early types (S0/a to Sab). Bulges with very low  $B/T$  ( $< 0.1$ ) lie primarily in lower mass galaxies with later morphologies (Sb to Sc). *It is striking that  $\sim 69\%$  of bright ( $M_B < -19.3$ ) moderately inclined spirals have  $B/T \leq 0.2$ : these bulges are pervasive and exist across the whole spectrum of S0/a to Sc.* The results are summarized in Table 7. We shall return to this point in § 5.8. We note again that these  $B/T$  mass ratios were calculated assuming a constant  $M/L$  ratio in the  $H$ -band for the bulge and disk components. As noted in § 5.2, if the bulge in these high mass spirals is much younger (older) than the disk and bar, then the  $B/T$  can be overestimated

(underestimated) by up to a factor of 2, and the limiting value of 0.2 for the  $B/T$  cited in the above fraction, would have to be modified in the extreme case to 0.1 and 0.4, respectively.

Some of the low  $B/T \leq 0.2$  values for six barred S0/a and Sa on Figure 12 may at first look suspicious. However, visual inspection of their images shown in (Figure 15) shows that the bulges do not seem very conspicuous compared to the disk, and suggests that the measured low  $B/T$  values are in fact reasonable. It is likely that these galaxies were assigned early Hubble types due to their smooth extended disks, although they have a low bulge-to-disk ratio. Similarly, some of the high  $B/T \sim 0.4$  value in three of the S0s may at first look odd. However, again, visual inspection of their image (Figure 15) suggests the large  $B/T$  are reasonable: these galaxies have large bulges relative to their disks. In fact, NGC 4647 has such a prominent bulge and smooth disk that it is unclear why it was assigned a late RC3 Hubble type : for all intents and purposes it looks like an Sa. The other two (NGC 3810 and 4254) galaxies have prominent bulges and nuclear spiral arms.

How does the bulge Sérsic index  $n$  vary as a function of Hubble type, and galaxy stellar mass (Figure 12), as well as  $B/T$  (Figure 13)? The results are summarized in Table 7. Only a small fraction ( $\sim 5\%$ ) of bright spirals have high  $n \geq 4$  bulges: such bulges lie primarily in S0/a to Sab, and have a large  $B/T > 0.2$ . A moderate fraction ( $\sim 35\%$ ) have intermediate  $2 < n < 4$  bulges: these exist in barred and unbarred S0/a to Sd, and their  $B/T$  spans a wide range (0.03 to 0.5) with a mean of 0.23. *A strikingly large fraction ( $\sim 60\%$ ) of bright spirals have low  $n \leq 2$  bulges: such bulges exist in barred and unbarred galaxies across all Hubble types, and their  $B/T$  ranges from 0.01 to 0.4, with most having  $B/T \leq 0.2$ .* Our results agree with those of Laurikainen et al. (2007), who find  $n \leq 2$  bulges across early and late Hubble type galaxies, in a sample that combines the present OSUBSGS sample with a sample of S0s. The prevalence of pseudobulges in galaxies of different Hubble types is also discussed in KK04, and select examples of S0s galaxies with pseudobulges are also shown in Kormendy & Cornell (2004) and KK04.

#### 5.4. Comparison With Independent Decompositions

As an independent check of our decomposition method, we compare our results with independently published decompositions.

Graham (2001) published 1D decompositions for 86 galaxies using optical and near-infrared light profiles. We find our mean  $H$ -band  $B/D$  (Figure 16) ratios are comparable to his  $K$ -band  $B/D$ . Like Graham (2001), we find  $B/D$  is widely variable with Hubble type and that mean  $B/D$  steadily declines from Sa through Scd galaxies. Graham (2001) finds bulge indices are widely scattered across Hubble type, but they are in general  $> 1$  for early types and  $< 1$  for late types. We likewise find wide scatter in bulge index with  $n < 1$  bulges existing in both early and late types.

Another meaningful comparison can be made with Laurikainen et al. (2007) who, using their own 2D decomposition code, fit a hybrid sample containing some OSUBSGS galaxies. One difference between their work and ours is that they typically model bars with a Ferrers function, but may sometimes use a Sérsic profile, while we only use the latter. Also, they include additional components to model secondary bars or inner disks. They report a distinct offset in the mean  $B/T$  between barred and unbarred galaxies, which we confirm in Figure 12. Their mean  $B/T$  are similar to ours, and they conclude that pseudobulges exist throughout the Hubble sequence. The Sérsic indices derived by Laurikainen et al. (2007) are slightly different from ours: there is good agreement in the mean index for barred galaxies, but the indices of our unbarred galaxies are larger. On the mean, we find unbarred Sa and Sb galaxies to have indices of  $\sim 3.25$ . Laurikainen

et al. (2007) find a mean index for unbarred galaxies of the same Hubble types to be  $\sim 2.25$ . The discrepancy still exists for Sc-Sd galaxies where our mean indices are slightly larger by  $\sim 0.5$ .

### 5.5. Bar Strength

Stellar bars exert gravitational torques on the gaseous component and are particularly efficient in driving gas from the outer disk into the inner kiloparsec (see § 1). Thus, it would be natural to have a measure of bar strength, which is sensitive to the strength of the gravitational torque, and hence measures both the shape and mass of the bar.

Many measures of bar strength have been formulated. The  $Q_b$  method of (Block et al. 2002; Buta et al. 2003; Buta et al. 2005) measures directly the gravitational torque at a single point along the bar. This method requires a scaleheight for the disk and a model of the potential to be made from the image. In the bar/interbar contrast method of Elmegreen & Elmegreen (1985) and Elmegreen et al. (1996), bar strength is parameterized as the ratio between peak surface brightness in the bar region and the minimum surface brightness in the interbar region. Elmegreen & Elmegreen (1985) and Elmegreen et al. (1996) also characterize bar strength with the maximum amplitude of the  $m = 2$  mode from Fourier decomposition. When ellipse fitting is applied, the maximum ellipticity of the bar,  $e_{bar}$ , can be used to characterize bar strength (e.g. MJ07). This constitutes only a partial measure of bar strength, however, as it offers no information about mass of the bar.

Bulge-disk-bar decomposition in the  $H$ -band provides another measure of bar strength through the  $H$ -band Bar/ $T$  light ratio. The latter is a measure of the Bar/ $T$  mass ratio, under the assumption that the  $H$ -band  $M/L$  ratio is the same for the bar and the rest of the galaxy, as discussed in § 5.2. Figures 17 and 18 explore the derived bar properties.

The upper left panel of Figure 17 plots the individual and mean Bar/ $T$  against Hubble type. There is a wide range ( $\sim 0.03$  to  $\sim 0.47$ ) in the individual Bar/ $T$  at a given Hubble type. The mean Bar/ $T$  remains fairly constant with Hubble type from Sa to Sb, but shows a possible weak decline by about 0.1 from Sb to Sc. There number statistics are too small to make any robust statement for later Hubble types. We also note that six systems have high Bar/ $T$  above 0.3: these are displayed in Figure 19.

Bar Sérsic indices are mostly below unity. Neither the individual, nor the mean bar Sérsic index, show any trend with Hubble type or with stellar mass, for Sa to Sc galaxies (Fig. 17). Thus, the steepness of the bar profile does not seem to depend on the Hubble type. Is the bar mass ratio and its mass profile related? There is a wide range in the individual Bar/ $T$  at a given bar Sérsic index (Fig. 18). The mean Bar/ $T$  rises with bar index out to a bar index of  $\sim 0.6$ , and then flattens out. This suggests that on the mean, bars of lower Bar/ $T$  have flatter profiles.

Is there a relation between the bar strength and the bulge present in a galaxy? There is a wide range in the individual Bar/ $T$  at a given  $B/T$ , and at a given bulge Sérsic index (Fig. 18). The mean Bar/ $T$  shows a weak decline for bulge Sérsic indices above 2. Similarly the mean Bar/ $T$  shows a weak rise from 0.1 to 0.25 as  $B/T$  rises out to 0.15, after which the trend flattens or reverses.

How do different measures of bar strength compare? The upper left panel of Figure 18 plots Bar/ $T$  against maximum bar ellipticity  $e_{bar}$ , as determined by MJ07 for galaxies mutually classified as barred. The bars with highest  $e_{bar}$  (i.e. thin bars) are often termed strong bars, and  $e_{bar}$  has been shown to correlate with  $Q_b$ . However, we find that there is a wide range in the individual Bar/ $T$  at a given  $e_{bar}$ , and the mean Bar/ $T$

does not rise for higher  $e_{bar}$ . Thus, the fractional mass ratio of bars appears to bear no relation to their shape (ellipticity). We note that bars with high Bar/T and high  $e_{bar}$  should exert the largest gravitational torque and be most effective at driving gas inflows. A nice example is the oval or lens galaxy NGC 1317 (Figure 19): the bar has a low ellipticity, but its  $B/T$  is large as it is extended and massive. Such bars/lenses may exert significant gravitational torques although they are not very elongated.

### 5.6. Bar Fraction as a Function of $B/T$ and Bulge Index

As outlined in § 5.3, we found that as many as  $59.6 \pm 4.06\%$  of bright spirals have bulges with  $n \leq 2$ : such bulges exist in barred and unbarred galaxies across all Hubble types, and their  $B/T$  ranges from 0.01 to 0.4, with most having  $B/T \leq 0.2$ . The variation of the bar fraction as a function of  $B/T$  and bulge  $n$  can provide important constraints on bulge formation scenarios (§ 5.8). Table 8 shows our results. The bar fraction declines with bulge index:  $\sim 64\%$  of the spirals with low  $n \leq 2$  bulges host bars. Intermediate  $2 < n < 4$  bulges have a slightly lower bar fraction ( $\sim 52\%$ ) while high  $n \geq 4$  bulges have the lowest bar fraction ( $\sim 29\%$ ). Similarly, systems with low  $B/T$  are more likely to be barred. For  $B/T \leq 0.2$ , the bar fraction is high ( $\sim 68\%$ ). Systems with  $0.2 < B/T < 0.4$  and  $B/T \geq 0.4$  have lower bar fraction ( $\sim 38\%$  and  $\sim 31\%$ ).

Overall, Table 8 shows that  $\sim 64\%$  of bright spirals with low  $n \leq 2$  bulges and  $\sim 68\%$  of bright spirals with low  $B/T \leq 0.2$  bulges host bars. *This suggests that in bright spirals, spontaneous or/and tidally induced bars may play a part in forming  $\sim$  two thirds low  $B/T \leq 0.2$  or low  $n \leq 2$  bulges. The remaining one third of such bulges may have been formed either by mechanisms that do not involve bars (e.g., retrograde minor mergers) or by bars that are not long-lived.*

### 5.7. Formation of Bulges

Our observational results provide some interesting challenges for models of galaxy evolution, which try to address the origin of present-day bulges. Any successful model must be able to account for the observed distribution of bulge  $B/T$  and  $n$  in high mass ( $M_\star \geq 1.0 \times 10^{10} M_\odot$ ) spirals, as shown in Table 7 and Table 8. In particular, the following results must be reproduced:

1. In terms of the overall distribution of bulge  $n$ , as much as ( $\sim 57\%$ ) of high mass spirals have bulge  $n \leq 2$ : such bulges exist in barred and unbarred galaxies and their  $B/T$  ranges from 0.01 to 0.4, with most having  $B/T \leq 0.2$  (Table 7). A moderate fraction ( $\sim 37\%$ ) of high mass spirals have  $2 < n < 4$ , and only ( $\sim 6\%$ ) have  $n \geq 4$ .
2. Theoretical models often make more robust predictions on the bulge-to-total mass ratio  $B/T$  than on the bulge index  $n$ , so we consider the empirical  $B/T$  distribution in detail. We note that as much as  $\sim 66\%$  of high mass spirals have bulges with  $B/T \leq 0.2$ , of which  $\sim 47\%$  have bulge  $n \leq 2$  (Table 7). In terms of bar fraction,  $\sim 68\%$  are barred (Table 8).
3. The fraction of bars rises among spirals with low bulge index  $n$ . About 64% of spirals with low  $n \leq 2$  bulges host bars, while the bar fraction in spirals with high  $n \geq 4$  bulges (29%) bulges is more than two times lower (Table 8).

In a hierarchical Universe, there are several physical processes that contribute to the assembly of bulges: major mergers, minor mergers, and secular evolution. We briefly describe these, expanding on our introduction in § 1.

Major mergers, typically defined as those with mass ratio  $M_1/M_2 \geq 1/4$ , destroy stellar disks during violent relaxation, leaving behind a classical bulge. Such bulges are associated with modest-to-high bulge Sérsic indices, in the range  $2 < n < 6$  (Hopkins et al. 2008, in prep.; Springel et al. 2005; Robertson et al. 2006; § 5.8) in simulations. This trend is also consistent with the fact that among ellipticals, high luminosity ones tend to have a Sérsic index  $n > 4$ , while low luminosity ones tend to have  $2 \leq n \leq 3.5$ . (Kormendy et al. 2008, in prep.). The final Sérsic index depends on the amount of residual gas the settles into a somewhat disk component. Simulations of Hopkins et al. (2008, in prep.) find that the Sérsic indices of a representative set of 1:1 major merger remnants lie in the range of  $2 < n < 4$ , with most above 2.5 (see Fig. 20). This body of evidence strongly suggests that many bulges with  $n > 2$  might have a major merger origin.

Minor mergers, typically defined as those with mass ratio  $1/10 < M_1/M_2 < 1/4$ , do not destroy the stellar disk of the primary system, but can contribute to building bulges via three pathways. Firstly, a fraction  $F_{sat}$  of the satellite’s stellar mass can end up in the central region of the primary galaxy. The value of  $F_{sat}$  depends on how centrally concentrated the infalling satellite is. Typically, the more diffuse outer stellar body is tidally stripped, while the central core sinks by dynamical friction to the central region (e.g., Quinn et al. 1993; Walker et al. 1996). Secondly, a bar can be induced in the main disk, and gravitational torques exerted by the bar can drive gas into the inner kpc (e.g., Quinn et al. 1993; Hernquist & Mihos 1995; Jogee 2006 and references therein), where subsequent SF forms a compact high  $v/\sigma$  stellar component, or disk pseudobulge. Most of the gas inflow happens during the merger phase and large gas inflow rates (e.g.,  $\gg 1 M_\odot$  per year) may be generated. Thirdly, gas inflow can also be caused by direct tidal torques from the companion (e.g., Hernquist & Mihos 1995). It is to be noted that in the simulations by Hernquist & Mihos (1995), the gas inflow caused by the induced bar is much larger than that caused by direct tidal torques from the satellite.

In addition, the process of secular evolution can build a disk bulge (pseudobulge) between merger events. Here a stellar bar or globally oval structure in a *non-interacting* galaxy drives gas inflow into the inner kpc, where subsequent SF forms a compact high  $v/\sigma$  stellar component (e.g., Kormendy 1993; Jogee 1999; KK04; Jogee, Scoville, & Kenney 2005; Athanassoula 2005; Kormendy & Fisher 2005). This process is different from that of minor mergers in the sense that it happens in the quiescent phase of the galaxy, between minor or major merger events.

Therefore, the present-day bulge mass can be written as the sum of mass contributed from each process:

$$M_{bulge} = M_{bulge} \times (f_{maj} + f_{min1} + f_{min2} + f_{min3} + f_{sec}), \quad (6)$$

where

- $f_{maj}$  is the percentage of the bulge stellar mass, which is built by major mergers,
- $f_{min1}$  is the percentage of the bulge stellar mass, which is built during minor mergers from stars of the satellite. This depends on the fraction  $F_{sat}$  of the satellite’s stellar mass, which ends up in the central region of the primary galaxy during each minor merger.
- $f_{min2}$  is the percentage of the bulge stellar mass built, which is from gas inflow during minor mergers caused by a tidally induced bar.

- $f_{\min 3}$  is the percentage of the stellar mass, which is built from gas inflow during minor mergers, caused by tidal torques from the companion.
- $f_{\sec}$  is the percentage of the stellar mass, which is built secularly from gas inflow between merger events caused by bars or ovals

In §5.8, we compare our derived distribution of bulge  $n$  and  $B/T$  to hierarchical models that model major and minor mergers, but not secular evolution. The main goal of the model is to see whether bulges built via major mergers can account for the large fraction of high mass spirals with bulges of low  $B/T$  or/and low  $n$ . A secondary goal is to see if a first order simplified prescription for minor mergers can broadly account for the observations. We stress here that bulge-building during minor mergers is modeled in a very simple way: all the stars in the satellite are assumed to contribute to the bulge of the larger galaxy (i.e.,  $F_{\text{sat}} = 100\%$ ), and bulge-building via gas inflow driven through tidal torques and via gravitational torques from induced bars are ignored (i.e.,  $f_{\min 2} = 0$ , and  $f_{\min 3} = 0$ ). Furthermore, the models entirely ignore secular evolution between mergers. In a future paper, these extra terms will be addressed and a comprehensive picture built of the relative importance of minor mergers and secular processes in making present-day bulges.

### 5.8. Comparison of $B/T$ With Hierarchical Models of Galaxy Evolution

We compare our data with the predictions from cosmological semi-analytical models based on Khochfar & Burkert (2005) and Khochfar & Silk (2006). We briefly describe the models first. The merger trees of dark matter (DM) halos are derived by using the extended Press-Schechter formalism (Press & Schechter 1974) to generate merger trees of dark matter halos (Somerville & Kolatt 1999). When two DM halos merge, the merger time scale of the galaxies is calculated considering the timescale it would take the satellite galaxies to reach the central galaxy at the center of the halo via dynamical friction (e.g., Kauffmann et al. 1999; Springel et al. 2001). The baryonic physics, which includes radiative cooling, star formation, and feedback from supernovae, is treated via semi-analytic prescriptions (see Khochfar & Silk (2006) and references therein). Baryonic mass inside the dark matter halos is divided between hot gas, cold gas, and stars. The hot gas is initially shock-heated to the halo virial temperature. As the gas radiatively cools, it settles down into a rotationally supported disk at the halo center. Cold disk gas is allowed to fragment and subsequently form stars according to the Schmidt-Kennicutt law (Kennicutt 1998). Star formation is regulated by feedback from supernovae using the prescription in Kauffmann et al. (1999).

Major mergers are typically considered as those with stellar mass ratio  $M_1/M_2 \geq 1/4$ . In the simulations, one assumes that during a major merger any existing stellar disk is destroyed, gas is converted to stars with some star formation efficiency (SFE), and all stars present undergo violent relaxation to form a bulge. Therefore, the bulge-to-total stellar mass ratio ( $B/T$ ) of a bulge immediately after a major merger is always one. Note that the SFE during a major merger is not assumed to be 100% as there is mounting evidence from SPH simulations (Springel & Hernquist 2005; Cox et al. 2008) that not all cold gas is converted to stars. Instead, the burst efficiency defined by Cox et al. (2008) is applied to control the fraction of stars formed due to the interaction. This efficiency is dependent on the relative masses of merging galaxies and is expressed as

$$e = e_{1:1} \left( \frac{M_{\text{Satellite}}}{M_{\text{Primary}}} \right)^\gamma, \quad (7)$$

where  $e_{1:1}$  is the burst efficiency for a 1:1 merger and  $\gamma$  fixes the dependence on mass ratio; Cox et al. (2008) find  $e_{1:1} = 0.55$  and  $\gamma = 0.69$ . The remaining fraction ( $1-e$ ) of gas is added to the gaseous disk and can start

making stars.

As stated above, immediately after a major merger, the remnant is a bulge with  $B/T$  equal to one. As time proceeds, the  $B/T$  falls because a stellar disk grows around the bulge as hot gas in the halo cools, settles into a disk, and forms stars. The formation of stars by any residual cold gas left at the end of the major merger also helps to grow the disk. Thus  $B/T$  falls until the next major merger happens, at which point  $B/T$  is reset to one in the models.

The bulge may also grow in stellar mass due to minor mergers. Minor mergers are defined as mergers with mass ratio  $1/10 < M_1/M_2 < 1/4$ , and the stellar disk of the large companion is not destroyed during such mergers. The models assume that during minor mergers, all the stars in the satellite are added to the bulge of the host, while the gas settles in the disk. When DM halos grow by accretion or minor mergers, the hot gas that comes in with a satellite is immediately stripped and added to the hot gas component of the host. The cold gas in the disk of the satellite is only added to the cold gas of the host if they merge. Until they merge the satellite is using up its own cold gas to make stars.

The galaxy merger histories can be extracted from the models. Only  $\sim 20\%$  of the galaxies experience *both* major and minor mergers over their lifetime (since  $z < 20$ ), while  $\sim 80\%$  experience *only* minor mergers. For galaxies that experienced a major merger, the  $B/T$  of the remnant at  $z \sim 0$  is plotted against the redshift  $z_{\text{last}}$  of the last major merger in Fig. 21. As expected, systems where the last major merger occurred at earlier times, have had more time to grow a disk and have a lower  $B/T$ . The dispersion in the present-day  $B/T$  at a given  $z_{\text{last}}$  is due to the different times spent by a galaxy in terms of being a satellite versus a central galaxy in a DM halo, since the cooling of gas and the growth of a disk is stopped when a galaxy becomes a satellite. Thus, galaxies that became a satellite galaxy shortly after their last major merger stayed at high  $B/T$ . Conversely, galaxies that continued to be a central galaxy for a long time after their last major merger will have low  $B/T$ .

The models imply that *a galaxy with a past major merger can have  $B/T \leq 0.2$  only if its last major merger occurred at  $z > 2$  (lookback times  $> 10$  Gyr)*. (Fig. 21). In the models, the fraction ( $\sim 3\%$ ; Table 9) of high mass spirals, which have undergone a past major merger and host a present-day bulge with  $B/T \leq 0.2$  is *a factor of over fifteen smaller* than the observed fraction ( $\sim 66\%$ ) of high mass spirals with  $B/T \leq 0.2$ . Thus, *bulges built via major mergers seriously fail to account for most of the low  $B/T \leq 0.2$  bulges present in  $\sim 66\%$  of high mass spirals*.

The majority of such bulges exist in systems that have experienced only minor mergers, and no major mergers. These bulges can in principle be built via minor mergers and secular processes, as described in § 5.7. However, the minor merger models shown here only explore bulge-building through the addition of all the satellite stars directly to the central region of the primary galaxy (see § 5.7). The results are shown in Fig. 22 and Table 9. The fraction of model galaxies where bulges are only built via minor mergers is  $B/T \leq 0.2$  is  $\sim 64\%$ , in good agreement with the observed fraction ( $\sim 66\%$ ) of high mass spirals with  $B/T \leq 0.2$ .

Since the results depend on the galaxy merger history in the models, it is legitimate to ask whether these are well-constrained observationally. Over the redshift range  $z \sim 0.24$  to  $0.80$  (lookback times of 3 to 7 Gyr), recent observational constraints on the rate of mergers of mass ratio  $> 1/10$  (i.e., major+minor mergers) among high mass galaxies (Jogee et al. 2008a,b) show agreement within a factor of  $\sim 2$  with the merger rates from these models (Khochfar & Burkert 2001).

How sensitive are the results to the model and data assumptions? We present below several tests:

- How sensitive are the results to the mass ratio used to separate major and minor mergers? Fig. 23 is

similar to Fig. 22 except that the model now defines major mergers as those with mass ratio  $M_1/M_2 \geq 1/6$ . In this case, about 30% of the model spirals undergo major mergers over their lifetime rather than  $\sim 20\%$ . The overall model  $F$  (black dashed line) now underpredicts the data  $F$  by about 10% for  $B/T > 0.2$ . However, the main conclusion that bulges built by major mergers cannot account for most of the low  $B/T \leq 0.2$  bulges, present in a large percentage ( $\sim 66\%$ ) of spirals still holds.

- How sensitive are the results to the  $B/T$  cut used to define spirals? Fig. 24 is similar to Fig. 22 except that here spirals are considered to be systems with a  $B/T \leq 0.55$  rather than 0.75 in the models, and a corresponding cut is applied to the data points. The results are similar to Fig. 22
- How sensitive are the results to the our assumed constant  $H$ -band mass-to-light ( $M/L$ ) for the bulge, disk and bar. Fig. 25 is similar to Fig. 22 except that the  $B/T$  of all the observed galaxies has been multiplied by a factor of two, in order to test what would happen in the case where the  $M/L$  ratio of the bulge in  $H$ -band is twice as high as that of the disk and bar. This could happen in an extreme example where the dominant bulge stellar population was much older (e.g. 12 Gyr) than the age of the dominant disk stellar population (e.g., 3 Gyr). In such a case the fraction of high mass spirals with  $B/T \leq 0.2$  would change from  $\sim 66\%$  in Fig. 22 to  $\sim 55\%$ , and deviate from the model overall model  $F$  (black dashed line) by  $\sim 20\%$ . However, the main conclusion that bulges built by major mergers cannot account for most of the low  $B/T \leq 0.2$  bulges, present in a large percentage ( $\sim 55\%$ ) of spirals still holds.

Finally it is important to note that so far we have only compared the data and model in terms of bulge  $B/T$ , but not in terms of bulge index  $n$  or in terms of bar fraction. In effect, we have only shown that the models reproduce a subset of the results outlined in points (1) (2) (3) of § 5.7. Since the semi-analytic models do not produce a distribution of bulge index  $n$ , we resort to presenting only an indirect comparison in Table 10. We assume that bulges, which form in major mergers have a bulge  $n > 2.5$ . This assumption is based on the evidence presented in § 5.7. Thus, in Test 1 of Table 10, we compare the fraction ( $64.09\% \pm 0.55\%$ ) of galaxies in the semi-analytic models having  $B/T \leq 0.2$  and no past major merger, to the observed fraction ( $57.5\% \pm 4.65\%$ ) of galaxies with  $B/T \leq 0.2$  and bulge  $n \leq 2.5$ . There is reasonable agreement within a factor of 1.2 between the two values. Similarly, in Test 2 of Table 10, the fraction ( $12.75\% \pm 0.38\%$ ) of model galaxies with  $B/T > 0.4$  and a past major merger compares within a factor of 1.8 with the fraction ( $7.08\% \pm 2.41\%$ ) of high mass spirals with  $B/T > 0.4$  and bulge  $n > 2.5$ . However, the fraction ( $3.09\% \pm 0.20\%$ ) of model galaxies with  $B/T \leq 0.2$  and a past major merger seems lower by a factor of  $\sim 3$  in the mean than the observed fraction ( $8.85\% \pm 2.67\%$ ) of high mass spirals with  $B/T \leq 0.2$  and bulge  $n > 2.5$  (Test 3, Table 10). A better agreement ( $3.54\% \pm 1.74\%$ ) is obtained in this case with a cutoff of  $n > 3$  in the data. Thus, these three indirect tests on whether the model and data agree in terms of bulge  $B/T$  and  $n$  work out well for Test 1 (model galaxies with no major mergers), but less well for Tests 2 and 3 (model galaxies with major mergers). Overall the picture that emerges is that *the vast majority of bulges with  $B/T \leq 0.2$  and  $n \leq 2.5$  are likely to form in galaxy having undergone only minor mergers*.

What about the role of bars in the formation of these bulges of low  $B/T$  and low  $n$ ? A detailed direct comparison with the semi-analytic models is not possible as the role of bars is not yet modeled, but related comparisons are possible. First, it is important to note that bar-driven gas inflow into the inner kpc and the subsequent building of disky stellar components or 'pseudobulges' (see § 1) can happen in both isolated galaxies and in minor merger (§ 5.7), since bars can be spontaneously induced in an isolated disk or tidally induced during an interaction or minor merger. The triggering of a bar is favored in a prograde interaction or minor merger. Thus, bulge-building via induced bars is more likely to happen in prograde rather than retrograde minor mergers. Statistically about half of minor mergers might be prograde or prograde-like, and half retrograde. Thus, one would expect bars to be induced in only half of the minor mergers. If this

assumption is correct and if most bulges with  $B/T \leq 0.2$  are formed in minor mergers, then one would expect only about half of these bulges to host bars. This is close to what is observed, as shown by Table 8. We see that  $\sim 64\%$  of high mass spirals with low  $n \leq 2$  bulges and  $\sim 68\%$  of spirals with low  $B/T \leq 0.2$  bulges host bars. *This suggests that in high mass spirals, spontaneous and/or tidally induced bars may play a part in forming  $\sim$  two thirds low  $B/T \leq 0.2$  or low low  $n \leq 2$  bulges. The remaining one third of such bulges may have been formed either by mechanisms that do not involve bars (e.g., retrograde minor mergers) or by bars that are not long-lived.*

## 6. Summary

The properties of galaxy components (bulges, disks, and bars) in the local Universe provide key constraints for models of galaxy evolution. Most previous  $2D$  decompositions have focused on two-component bulge-disk decomposition, and ignored the contribution of the bar even in strongly barred galaxies. However, as shown by this work and other recent studies (e.g., Laurikainen et al. 2005; Laurikainen et al. 2007; Reese et al. 2007), it is important to include the bar component in the  $2D$  decomposition, in order to correctly estimate the bulge-to-total ratio ( $B/T$ ) and disk properties. In this paper we have developed an iterative  $2D$ , bulge-disk-bar decomposition technique using GALFIT and applied it to  $H$ -band images to a complete sample (S1) of 146 bright ( $M_B < -19.3$ ) moderately inclined ( $i \leq 70^\circ$ ) spirals from the OSU Bright Spiral Galaxy Survey (OSUBSGS). The sample has primarily spirals with Hubble type S0/a to Sc and stellar mass  $M_* \geq 1.0 \times 10^{10} M_\odot$ . We performed two-component bulge-disk decomposition, as well as three-component bulge-disk-bar decomposition on the  $2D$  light distribution of all galaxies, taking into account the PSF. We use an exponential profile for the disk, and Sérsic profiles for the bulge and bar. A number of quantitative indicators, including bar classification from ellipse fits, are used to pick either the bulge-disk-bar decomposition or bulge-disk decomposition, as the best final fit for a galaxy. Our main results are the following.

1. We find that it is necessary to include the bar component in  $2D$  decomposition of barred galaxies, otherwise, the bulge-to-total ratio ( $B/T$ ) will be overestimated and the disk properties may be skewed. Examples of the effect of including the bar are shown for the prominently barred galaxies NGC 4643 (Figure 5, Table 2) and NGC 4548 (Figure 6, Table 3).
2. We find that out of the 146 moderately inclined spirals ( $i \leq 70^\circ$ ) in our sample, 77/146 or  $\sim 53\%$  are better fit with a Stage 3 bulge-disk-bar decomposition than a Stage 2 bulge-disk decomposition. There are also eight galaxies with pure bar-disk fits. The resulting  $H$ -band bar fraction, defined as the fraction of disk galaxies that are barred, is  $58.2 \pm 4.08\%$  (85/146). This fraction is in excellent agreement with the  $H$ -band bar fraction of 60% reported by MJ07, based on ellipse fits of the same OSUBSGS sample, with a more conservative inclination cut ( $i \leq 60^\circ$ ).
3.  $H$ -band images tend to trace the overall mass fairly well and are not overly impacted by extinction and age gradients. We therefore assume a constant mass-to-light ( $M/L$ ) in the  $H$ -band for the bulge, disk, and bar, and assume their  $H$ -band light fraction is a measure of their mass fraction. For our sample S1 of 146 bright ( $M_B < -19.3$ ) moderately inclined ( $i \leq 70^\circ$ ) spirals, we find that 69.9% of the stellar mass is in disks, 9.9% is in stellar bars and 20.2% is in bulges (with 15.5% in  $n > 2$  bulges and 4.7% in  $n \leq 2$  bulges).

If the bulge is younger than the disk and happens to harbor a significant young population of massive stars, then our prescription will *overestimate* the true  $B/T$  mass ratio, and make our current results

on the high fraction of low  $B/T$  bulges (see point 4 below) even stronger. On the other hand, if we assume an extreme case where disk are much younger (e.g.,  $\sim 3$  Gyr old) than bulges (e.g.,  $\sim 12$  Gyr old), then our prescription would underestimate the true  $B/T$  by a factor of  $\leq 2$ .

4. We explore the relationship between  $B/T$ , bulge Sérsic index, and Hubble types (Fig. 12 & Fig. 13). Only a small fraction ( $\sim 5\%$ ) of bright spirals have high  $n \geq 4$  bulges: such bulges lie primarily in S0/a to Sab, and have a large  $B/T > 0.2$ . A moderate fraction ( $\sim 35\%$ ) have intermediate  $2 < n < 4$  bulges: these exist in barred and unbarred S0/a to Sd, and their  $B/T$  spans a wide range (0.03 to 0.5) with a mean of 0.23. Finally, *a strikingly large fraction ( $\sim 60\%$ ) of bright spirals have low  $n \leq 2$  bulges: such bulges exist in barred and unbarred galaxies across all Hubble types, and their  $B/T$  ranges from 0.01 to 0.4, with most having  $B/T \leq 0.2$ .*
5. Bulges with very high  $B/T$  ( $> 0.4$ ) exist primarily in galaxies with high mass ( $M_* > 6 \times 10^{10} M_\odot$ ) and early types (S0/a to Sab). Bulges with very low  $B/T$  ( $< 0.1$ ) lie primarily in lower mass galaxies with later morphologies (Sb to Sc). *As many as  $\sim 69\%$  of bright spirals have bulges with  $B/T \leq 0.2$ : these bulges are pervasive and exist across the whole spectrum of S0/a to Scd* (Figure 12).
6. Modeling bars with 2D decomposition also allows us to measure bar properties and the bar-to-total ratio (Bar/ $T$ ), which is a measure of bar strength. There is a wide range ( $\sim 0.03$  to  $\sim 0.47$ ) in the individual Bar/ $T$  at a given Hubble type. The mean Bar/ $T$  remains fairly constant with Hubble type from Sa to Sb, but shows a possible weak decline by about 0.1 from Sb to Sc (See Figure 17 and Figure 18). The bar fraction (Table 8) declines with  $B/T$ : it is highest ( $\sim 68\%$ ) for spirals with  $B/T \leq 0.2$ , and lower ( $\sim 36\%$ ) by nearly a factor of two in spirals with  $B/T > 0.2$ .
7. We discuss the role of bars in the formation of these bulges of low  $B/T$  and low  $n$ . It is important to note that bar-driven gas inflow into the inner kpc and the subsequent building of disky stellar components or 'pseudobulges' can happen in both isolated galaxies and in minor mergers, since bars can be spontaneously induced in an isolated disk or tidally induced during an interaction or minor merger. The triggering of a bar is favored in a prograde interaction or minor merger. *Overall, we find that  $\sim 64\%$  of bright spirals with low  $n \leq 2$  bulges and  $\sim 68\%$  of bright spirals with low  $B/T \leq 0.2$  bulges host bars.* This suggests that spontaneous and tidally-induced bars may play a part in forming a large fraction of such bulges. The remaining one third of such bulges may have been formed either by mechanisms that do not involve bars (e.g., retrograde minor mergers) or by bars that are not long-lived.
8. We compare the observed distribution of bulge  $B/T$  and  $n$  in high mass ( $M_* \geq 1.0 \times 10^{10} M_\odot$ ) spirals with predictions from  $\Lambda$ CDM cosmological semi-analytical models (Figs. 22 to 25). Major mergers are considered as those with stellar mass ratio  $M_1/M_2 \geq 1/4$ . The model merger history shows that only  $\sim 20\%$  of the galaxies experience *both* major and minor mergers over their lifetime, while  $\sim 80\%$  experience minor mergers. In the models, a bulge with  $B/T \leq 0.2$  can exist in a galaxy with a past major merger, only if the last major merger occurred at  $z > 2$  (lookback time  $> 10$  Gyr; Fig. 21). In the models, the fraction ( $\sim 3\%$ ) of high mass spirals which have undergone a past major merger and host a present-day bulge with  $B/T \leq 0.2$  is *a factor of over fifteen smaller* than the observed fraction ( $\sim 66\%$ ) of high mass spirals with  $B/T \leq 0.2$ . Thus, *bulges built via major mergers seriously fail to account for most of the low  $B/T \leq 0.2$  bulges present in over 60% of high mass spirals.* The majority of such bulges exist in systems that have experienced only minor mergers, and no major mergers. Overall the picture that emerges is that *the vast majority of bulges with  $B/T \leq 0.2$  and  $n \leq 2.5$  are likely to form in galaxies that have experienced only minor mergers.* These bulges can be built via minor

mergers and secular processes. In this paper, we explore one realization of the model focusing on bulges built via satellite stars in minor merger and find good agreement with the observations. Future models will explore secular processes.

S.J. and T.W. acknowledge support from the National Aeronautics and Space Administration (NASA) LTSA grant NAG5-13063, NSF grant AST-0607748, and *HST* grants GO-10395 and GO-10861 from STScI, which is operated by AURA, Inc., for NASA, under NAS5-26555. We thank Chien Peng for technical assistance in the operation of GALFIT. We acknowledge the usage of the Hyperleda database (<http://leda.univ-lyon1.fr>). This research has made use of the NASA/IPAC Extragalactic Database (NED) which is operated by the Jet Propulsion Laboratory, California Institute of Technology, under contract with the National Aeronautics and Space Administration.

## REFERENCES

Allen, P. D., Driver, S. P., Graham, A. W., Cameron, E., Liske, J., & de Propris, R. 2006, MNRAS, 371, 2

Athanassoula, E. 2002, ApJL, 569, L83

Athanassoula, E. 2003, MNRAS, 341, 1179

Athanassoula, E. 2005, MNRAS, 358, 1477

Barazza, F. D., Jogee, S., & Marinova, I. 2007, IAU Symposium, 235, 76

Barazza, F. D., Jogee, S., & Marinova, I. 2008, ApJ, 675, 1194

Barrett, P. E., & Bridgman, W. T. 1999, Astronomical Data Analysis Software and Systems VIII, 172, 483

Bell, E. F., McIntosh, D. H., Katz, N., & Weinberg, M. D. 2003, ApJS, 149, 289

Berentzen, I., Shlosman, I., & Jogee, S. 2006, ApJ, 637, 582

Blanton, M. R., Lupton, R. H., Schlegel, D. J., Strauss, M. A., Brinkmann, J., Fukugita, M., & Loveday, J. 2005, ApJ, 631, 208

Block, D. L., Bournaud, F., Combes, F., Puerari, I., & Buta, R. 2002, A&A, 394, L35

Böker, T., Laine, S., van der Marel, R. P., Sarzi, M., Rix, H.-W., Ho, L. C., & Shields, J. C. 2002, AJ, 123, 1389

Bureau, M., & Athanassoula, E. 2005, ApJ, 626, 159

Burkert, A. M., & D'Onghia, E. 2004, Penetrating Bars Through Masks of Cosmic Dust, 319, 341

Burkert, A., & Naab, T. 2004, Coevolution of Black Holes and Galaxies, 421

Buta, R., Block, D. L., & Knapen, J. H. 2003, AJ, 126, 1148

Buta, R., Vasylyev, S., Salo, H., & Laurikainen, E. 2005, AJ, 130, 506

Byun, Y. I., & Freeman, K. C. 1995, ApJ, 448, 563

Charlot, S. 1996, The Universe at High- $z$ , Large-Scale Structure and the Cosmic Microwave Background, 470, 53

Charlot, S., Worthey, G., & Bressan, A. 1996, ApJ, 457, 625

Cole, S., Lacey, C. G., Baugh, C. M., & Frenk, C. S. 2000, MNRAS, 319, 168

Combes, F., & Sanders, R. H. 1981, A&A, 96, 164

Combes, F., Debbasch, F., Friedli, D., & Pfenniger, D. 1990, A&A, 233, 82

Cox, T. J., Jonsson, P., Somerville, R. S., Primack, J. R., & Dekel, A. 2008, MNRAS, 384, 386

Debattista, V. P., & Sellwood, J. A. 1998, ApJL, 493, L5

Debattista, V. P., & Sellwood, J. A. 2000, ApJ, 543, 704

Drory, N., Bender, R., & Hopp, U. 2004, ApJL, 616, L103

de Jong, R. S. 1996, A&A Suppl., 118, 557

de Souza, R. E., Gadotti, D. A., & dos Anjos, S. 2004, ApJS, 153, 411

de Vaucouleurs, G., de Vaucouleurs, A., Corwin, H. G., Jr., Buta, R. J., Paturel, G., & Fouque, P. 1991, Volume 1-3, XII, 2069 pp. 7 figs.. Springer-Verlag Berlin Heidelberg New York

D’Onghia, E., Burkert, A., Murante, G., & Khochfar, S. 2006, MNRAS, 372, 1525

Driver, S. P., Liske, J., Cross, N. J. G., De Propris, R., & Allen, P. D. 2005, MNRAS, 360, 81

Driver, S. P., et al. 2006, MNRAS, 368, 414

Efstathiou, G., Ellis, R. S., & Peterson, B. A. 1988, MNRAS, 232, 431

Elmegreen, B. G., & Elmegreen, D. M. 1985, ApJ, 288, 438

Elmegreen, B. G. 1994, ApJL, 425, L73

Elmegreen, B. G., Elmegreen, D. M., Chromey, F. R., Hasselbacher, D. A., & Bissell, B. A. 1996, AJ, 111, 2233

Eskridge, P. B., et al. 2000, AJ, 119, 536

Eskridge, P. B., et al. 2002, ApJS, 143, 73

Fisher, D., & Drory N. 2008, AJ, accepted

Gadotti, D., & Kauffmann, G. 2007, IAU Symposium, 241, 507

Graham, A. W. 2001, AJ, 121, 820

Hernquist, L. & Mihos, J. C. 1995, ApJ, 448, 41

Ho, L. C., Filippenko, A. V., & Sargent, W. L. W. 1997, ApJS, 112, 315

Hunt, L. K., & Malkan, M. A. 1999, ApJ, 516, 660

Jogee, S., Kenney, J. D. P., & Smith, B. J. 1999, ApJ, 526, 665

Jogee, S. 1999, Ph.D. Thesis,

Jogee, S., et al. 2004, ApJL, 615, L105

Jogee, S., Scoville, N., & Kenney, J. D. P. 2005, ApJ, 630, 837

Jogee, S. 2006, Physics of Active Galactic Nuclei at all Scales, 693, 143

Jogee, S. et al. 2008a, in Formation and Evolution of Galaxy Disks, ed. J. G. Funes, S. J., & E. M. Corsini (San Francisco: ASP), in press (arXiv:0802.3901)

Jogee, S., et al. 2008b, ApJ, submitted

Kauffmann, G., Colberg, J. M., Diaferio, A., & White, S. D. M. 1999, MNRAS, 303, 188

Kauffmann, G., et al. 2003, MNRAS, 341, 33

Kautsch, S. J., Grebel, E. K., Barazza, F. D., & Gallagher, J. S., III 2006, A&A, 445, 765

Kennicutt, R. C., Jr. 1998, ApJ, 498, 541

Khochfar, S., & Burkert, A. 2001, ApJ, 561, 517

Khochfar, S., & Burkert, A. 2005, MNRAS, 359, 1379

Khochfar, S., & Silk, J. 2006, MNRAS, 370, 902

Knapen, J. H., Beckman, J. E., Heller, C. H., Shlosman, I., & de Jong, R. S. 1995, ApJ, 454, 623

Knapen, J. H., Shlosman, I., & Peletier, R. F. 2000, ApJ, 529, 93

Koda, J., Milosavljevic, M., & Shapiro, P. R. 2007, ArXiv e-prints, 711, arXiv:0711.3014

Kormendy, J. 1993, in IAU Symposium 153, Galactic Bulges, ed. H. Dejonghe & H. J. Habing (Dordrecht: Kluwer), 209

Kormendy, J., & Cornell, M. E. 2004, Penetrating Bars Through Masks of Cosmic Dust, 319, 261

Kormendy, J., & Kennicutt, R. C., Jr. 2004, ARAA, 42, 603 (KK04)

Kormendy, J., & Fisher, D. B. 2005, Rev. Mex. AA Ser. Conf., 23, 101 (astro-ph/0507525)

Kormendy, J. 2008, in IAU Symposium 245, Formation and Evolution of Galaxy Bulges, ed. M. Bureau et al. (Cambridge: Cambridge Univ. Press), in press (astro-ph/0708.2104)

Kroupa, P., Tout, C. A., & Gilmore, G. 1993, MNRAS, 262, 545

Laine, S., Shlosman, I., Knapen, J. H., & Peletier, R. F. 2002, ApJ, 567, 97

Laurikainen, E., Salo, H., & Buta, R. 2004, ApJ, 607, 103

Laurikainen, E., Salo, H., & Buta, R. 2005, MNRAS, 362, 1319

Laurikainen, E., Salo, H., Buta, R., & Knapen, J. H. 2007, MNRAS, 381, 401

Liske, J., Lemon, D. J., Driver, S. P., Cross, N. J. G., & Couch, W. J. 2003, MNRAS, 344, 307

Marinova, I., & Jogee, S. 2007, ApJ, 659, 1176

Martinez-Valpuesta, I., Shlosman, I., & Heller, C. 2006, ApJ, 637, 214

Menéndez-Delmestre, K., Sheth, K., Schinnerer, E., Jarrett, T. H., & Scoville, N. Z. 2007, ApJ, 657, 790

Mihos, J. C., & Hernquist, L. 1996, ApJ, 464, 641

Mulchaey, J. S., & Regan, M. W. 1997, ApJL, 482, L135

Naab, T., & Burkert, A. 2001, ApJL, 555, L91

Naab, T., & Burkert, A. 2003, ApJ, 597, 893

Navarro, J. F., & Steinmetz, M. 2000, ApJ, 538, 477

Paturel G., Petit C., Prugniel P., Theureau G., Rousseau J., Brouty M., Dubois P., Cambrésy L., 2003, *A&A*, 412, 45

Peng, C. Y., Ho, L. C., Impey, C. D., & Rix, H.-W. 2002, *AJ*, 124, 266

Pfenniger, D., & Norman, C. 1990, *ApJ*, 363, 391

Press, W. H., & Schechter, P. 1974, *ApJ*, 187, 425

Reese, A. S., Williams, T. B., Sellwood, J. A., Barnes, E. I., & Powell, B. A. 2007, *AJ*, 133, 2846

Robertson, B., Yoshida, N., Springel, V., & Hernquist, L. 2004, *ApJ*, 606, 32

Robertson, B., Bullock, J. S., Cox, T. J., Di Matteo, T., Hernquist, L., Springel, V., & Yoshida, N. 2006, *ApJ*, 645, 986

Schechter, P. 1976, *ApJ*, 203, 297

Sheth, K., et al. 2008, *ApJ*, 675, 1141

Simard, L. 1998, *Astronomical Data Analysis Software and Systems VII*, 145, 108

Simard, L., et al. 2002, *ApJS*, 142, 1

Somerville, R. S., & Kolatt, T. S. 1999, *MNRAS*, 305, 1

Springel, V., White, S. D. M., Tormen, G., & Kauffmann, G. 2001, *MNRAS*, 328, 726

Springel, V., Di Matteo, T., & Hernquist, L. 2005, *MNRAS*, 361, 776

Springel, V., & Hernquist, L. 2005, *ApJL*, 622, L9

Steinmetz, M., & Navarro, J. F. 2002, *New Astronomy*, 7, 155

Quinn, P. J., Hernquist, L., & Fullagar, D. P. 1993, *ApJ*, 403, 74

Véron-Cetty, M.-P., & Véron, P. 2006, *A&A*, 455, 773

Wadadekar, Y., Robbason, B., & Kembhavi, A. 1999, *AJ*, 117, 1219

Walker, I. R., Mihos, J. C., & Hernquist, L. 1996, *ApJ*, 460, 121

Warren, S. J., et al. 2007, *MNRAS*, 375, 213

Weinberg, M. D. 1985, *MNRAS*, 213, 451

Table 1. Sample S1 of Bright ( $M_B < -19.3$ ) Moderately Inclined ( $i \leq 70^\circ$ ) Spirals in OSUBSGS (N=146)

Galaxy Name (1)	Best Fit (2)	Hubble Type (RC3) (3)	Bar Type (RC3) (4)	$D$ (Mpc) (5)	$M_B$ (mag) (6)	$B - V$ (mag) (7)	$M_\star$ ( $M_\odot$ ) (8)
ESO138-10	PSF+Bulge+Disk	SA(s)cd	A	16.35	-	-	-
IC0239	Bulge+Disk+Bar	SAB(rs)cd	AB	12.91	-19.10	0.70	1.34e+10
IC4444	Bulge+Disk	SAB(rs)bc	AB	27.83	-20.23	0.64	4.35e+10
IC5325	PSF+Bulge+Disk	SAB(rs)bc	AB	21.40	-19.83	0.56	9.78e+09
NGC0150	PSF+Bulge+Disk+Bar	SAB(rs)bc	B	21.76	-19.70	0.64	2.17e+10
NGC0157	Bulge+Disk	SAB(rs)bc	AB	24.72	-20.97	0.59	5.81e+10
NGC0210	Bulge+Disk+Bar	SAB(s)b	AB	24.78	-20.38	0.71	3.77e+10
NGC0278	Bulge+Disk	SAB(rs)b	AB	8.88	-18.27	0.64	1.24e+10
NGC0289	Bulge+Disk+Bar	SAB(rs)bc	AB	24.14	-20.20	0.73	3.33e+10
NGC0428	Bulge+Disk+Bar	SAB(s)m	AB	14.93	-18.96	0.44	5.28e+09
NGC0488	Bulge+Disk	SA(r)b	A	31.90	-21.38	0.87	2.44e+11
NGC0578	PSF+Bulge+Disk+Bar	SAB(rs)c	AB	22.81	-20.36	0.51	1.87e+10
NGC0613	Bulge+Disk+Bar	SB(rs)bc	B	21.57	-20.95	0.68	4.92e+10
NGC0685	Bar+Disk	SAB(r)c	AB	21.57	-19.96	0.46	5.47e+09
NGC0779	Bulge+Disk+Bar	SAB(r)b	AB	20.33	-19.60	0.79	3.64e+10
NGC0864	PSF+Bulge+Disk+Bar	SAB(rs)c	AB	22.14	-20.33	0.55	2.31e+10
NGC0908	PSF+Bulge+Disk	SA(s)c	A	24.30	-21.11	0.65	6.60e+10
NGC1042	PSF+Bulge+Disk	SAB(rs)cd	AB	20.10	-19.96	0.54	1.63e+10
NGC1058	PSF+Bulge+Disk	SA(rs)c	A	7.03	-17.42	0.62	4.74e+09
NGC1073	PSF+Bulge+Disk+Bar	SB(rs)c	B	17.27	-19.72	0.50	1.04e+10
NGC1084	PSF+Bulge+Disk	SA(s)c	A	20.20	-20.22	0.58	2.64e+10
NGC1087	Bar+Disk	SAB(rs)c	AB	20.20	-20.21	0.52	2.09e+10
NGC1187	PSF+Bulge+Disk+Bar	SB(r)c	B	22.08	-20.39	0.56	1.66e+10
NGC1241	Bulge+Disk+Bar	SB(rs)b	B	56.27	-21.78	0.85	2.05e+11
NGC1300	Bulge+Disk+Bar	SB(rs)bc	B	22.74	-20.68	0.68	5.39e+10
NGC1302	PSF+Bulge+Disk+Bar	(R)SB(r)0	B	24.72	-20.37	0.89	6.37e+10
NGC1309	Bulge+Disk	SA(s)bc	A	32.24	-20.58	0.44	1.46e+10
NGC1317	Bulge+Disk+Bar	SAB(r)a	AB	27.73	-20.31	0.89	6.42e+10
NGC1350	Bulge+Disk+Bar	(R')SB(r)ab	B	26.52	-20.97	0.87	1.38e+11
NGC1371	Bulge+Disk+Bar	SAB(rs)a	AB	20.77	-	-	-
NGC1385	Bar+Disk	SB(s)cd	B	20.77	-20.82	0.51	1.61e+10
NGC1511	Bulge+Disk	SAa;pec	A	19.06	-19.53	0.57	1.15e+10
NGC1559	Bar+Disk	SB(s)cd	B	19.06	-20.41	0.35	9.33e+09
NGC1637	PSF+Bulge+Disk+Bar	SAB(rs)c	AB	10.14	-18.56	0.64	4.70e+09
NGC1703	Bulge+Disk	SB(r)b	B	21.80	-19.80	0.56	8.43e+09
NGC1792	Bulge+Disk	SA(rs)bc	A	17.40	-20.34	0.68	3.71e+10
NGC1808	Bulge+Disk+Bar	(R)SAB(s)a	AB	14.49	-20.07	0.81	3.57e+10
NGC1964	PSF+Bulge+Disk+Bar	SAB(s)b	AB	24.27	-20.35	0.77	6.54e+10
NGC2090	Bulge+Disk+Bar	SA(rs)c	A	13.17	-19.15	0.79	1.90e+10
NGC2139	Bulge+Disk	SAB(rs)cd	AB	26.11	-20.10	0.36	8.35e+09
NGC2196	PSF+Bulge+Disk	(R')SA(s)a	A	32.87	-20.77	0.81	9.22e+10
NGC2442	Bulge+Disk+Bar	SAB(s)bc;pec	AB	19.98	-20.27	0.82	8.28e+10
NGC2559	Bulge+Disk+Bar	SB(s)bc;pec	B	22.29	-	-	-
NGC2566	Bulge+Disk	(R')SB(rs)ab;pec	B	23.40	-21.75	0.81	6.98e+10
NGC2775	PSF+Bulge+Disk	SA(r)ab	A	19.14	-20.39	0.90	9.46e+10
NGC3059	Bar+Disk	SB(rs)c	B	19.14	-19.64	0.68	2.52e+10
NGC3166	Bulge+Disk+Bar	SAB(rs)0	AB	18.94	-20.07	0.93	7.41e+10
NGC3169	Bulge+Disk	SA(s)a;pec	A	18.01	-20.20	0.85	6.09e+10
NGC3223	Bulge+Disk	SA(s)b	A	41.23	-21.30	0.82	2.36e+11
NGC3227	PSF+Bulge+Disk+Bar	SAB(s)a;pec	AB	18.89	-19.97	0.82	4.42e+10
NGC3261	Bulge+Disk+Bar	SB(rs)b	B	36.64	-	-	-
NGC3275	Bulge+Disk+Bar	SB(r)ab	B	45.87	-	-	-
NGC3319	Bar+Disk	SB(rs)cd	B	45.87	-18.73	0.41	4.76e+09

Table 1—Continued

Galaxy Name (1)	Best Fit (2)	Hubble Type (RC3) (3)	Bar Type (RC3) (4)	$D$ (Mpc) (5)	$M_B$ (mag) (6)	$B - V$ (mag) (7)	$M_\star$ ( $M_\odot$ ) (8)
NGC3338	PSF+Bulge+Disk+Bar	SA(s)c	A	18.53	-19.70	0.59	2.67e+10
NGC3423	Bulge+Disk	SA(s)cd	A	11.93	-18.80	0.45	5.89e+09
NGC3504	Bulge+Disk+Bar	(R)SAB(s)ab	AB	21.69	-19.87	0.72	4.06e+10
NGC3513	Bulge+Disk+Bar	SB(rs)c	B	17.00	-19.23	0.43	7.52e+09
NGC3583	Bulge+Disk+Bar	SB(s)b	B	30.54	-	-	-
NGC3596	PSF+Bulge+Disk	SAB(rs)c	AB	16.80	-	-	-
NGC3646	PSF+Bulge+Disk	Ring	-	60.87	-22.16	0.65	2.82e+11
NGC3675	PSF+Bulge+Disk	SA(s)b	A	10.34	-	-	-
NGC3684	Bulge+Disk	SA(rs)bc	A	19.92	-19.50	0.62	1.00e+10
NGC3686	Bulge+Disk+Bar	SB(s)bc	B	14.76	-18.96	0.57	9.97e+09
NGC3705	Bulge+Disk+Bar	SAB(r)ab	AB	15.06	-19.03	0.79	3.15e+10
NGC3726	Bulge+Disk+Bar	SAB(r)c	AB	13.54	-19.75	0.49	1.93e+10
NGC3810	PSF+Bulge+Disk	SA(rs)c	A	13.68	-19.34	0.58	1.72e+10
NGC3885	PSF+Bulge+Disk	SA(s)0	A	27.40	-20.31	0.95	4.62e+10
NGC3887	Bulge+Disk+Bar	SB(r)bc	B	17.27	-	-	-
NGC3893	Bulge+Disk	SAB(rs)c	AB	13.49	-	-	-
NGC3938	Bulge+Disk	SA(s)c	A	11.01	-19.31	0.52	1.23e+10
NGC3949	PSF+Bulge+Disk	SA(s)bc	AB	9.73	-18.40	0.45	8.66e+09
NGC4027	Bar+Disk	SB(s)dm	B	9.73	-20.20	0.54	2.25e+10
NGC4030	Bulge+Disk	SA(s)bc	A	20.94	-	-	-
NGC4051	PSF+Bulge+Disk+Bar	SAB(rs)bc	AB	9.83	-19.14	0.65	1.95e+10
NGC4062	Bulge+Disk	SA(s)c	A	10.60	-18.23	0.76	2.07e+10
NGC4123	PSF+Bulge+Disk+Bar	SB(r)c	B	17.69	-19.26	0.61	1.50e+10
NGC4145	PSF+Bulge+Disk	SAB(rs)d	AB	13.21	-18.83	0.51	1.34e+10
NGC4151	PSF+Bulge+Disk+Bar	(R')SAB(rs)ab	AB	13.66	-19.18	0.73	2.93e+10
NGC4212	Bulge+Disk	SAc	A	1.16	-13.48	0.67	3.28e+10
NGC4254	Bulge+Disk	SA(s)c	A	34.41	-22.25	0.57	1.61e+11
NGC4293	PSF+Bulge+Disk+Bar	(R)SB(s)0	B	10.24	-18.80	0.90	5.94e+10
NGC4303	Bulge+Disk+Bar	SAB(rs)bc	AB	22.96	-21.63	0.53	6.76e+10
NGC4314	Bulge+Disk+Bar	SB(rs)a	B	13.76	-19.27	0.85	3.69e+10
NGC4394	Bulge+Disk+Bar	(R)SB(r)b	B	11.03	-18.48	0.85	2.61e+10
NGC4414	PSF+Bulge+Disk+Bar	SA(rs)c	A	10.23	-19.09	0.84	4.38e+10
NGC4450	PSF+Bulge+Disk+Bar	SA(s)ab	A	27.93	-21.49	0.82	2.22e+11
NGC4487	Bulge+Disk+Bar	SAB(rs)cd	AB	14.78	-	-	-
NGC4490	Bulge+Disk	SB(s)d;pec	B	8.49	-19.43	0.43	4.10e+10
NGC4527	Bulge+Disk+Bar	SAB(s)bc	AB	24.67	-20.59	0.86	1.87e+11
NGC4548	PSF+Bulge+Disk+Bar	SB(rs)b	B	6.95	-18.42	0.81	7.85e+10
NGC4593	PSF+Bulge+Disk+Bar	(R)SB(rs)b	B	38.57	-	-	-
NGC4618	PSF+Bar+Disk	SB(rs)m	B	38.57	-18.23	0.44	4.62e+09
NGC4643	Bulge+Disk+Bar	SB(rs)0	B	19.98	-19.79	0.96	6.49e+10
NGC4647	Bulge+Disk	SAB(rs)c	AB	20.30	-19.60	0.65	1.67e+10
NGC4651	PSF+Bulge+Disk	SA(rs)c	A	11.26	-18.87	0.57	1.05e+10
NGC4654	Bulge+Disk	SAB(rs)cd	AB	14.95	-20.13	0.60	2.99e+10
NGC4665	Bulge+Disk+Bar	SB(s)0	B	11.22	-	-	-
NGC4689	Bulge+Disk	SA(rs)bc	A	21.74	-20.09	0.65	3.84e+10
NGC4691	Bulge+Disk+Bar	(R)SB(s)0;pec	B	15.83	-19.34	0.58	1.04e+10
NGC4698	Bulge+Disk	SA(s)ab	A	14.74	-19.39	0.91	5.15e+10
NGC4699	Bulge+Disk+Bar	SAB(rs)b	AB	21.12	-21.22	0.89	2.06e+11
NGC4772	PSF+Bulge+Disk+Bar	SA(s)a	A	14.87	-18.91	0.92	3.30e+10
NGC4775	Bulge+Disk	SA(s)d	A	22.41	-	-	-
NGC4781	Bulge+Disk	SB(rs)d	B	18.01	-	-	-
NGC4818	PSF+Bulge+Disk+Bar	SAB(rs)ab;pec	AB	15.36	-18.94	0.89	3.88e+10
NGC4856	Bulge+Disk+Bar	SB(s)0	B	17.87	-19.78	0.99	9.04e+10

Table 1—Continued

Galaxy Name (1)	Best Fit (2)	Hubble Type (RC3) (3)	Bar Type (RC3) (4)	D (Mpc) (5)	$M_B$ (mag) (6)	$B - V$ (mag) (7)	$M_*$ ( $M_\odot$ ) (8)
NGC4902	Bulge+Disk+Bar	SB(r)b	B	38.93	-21.36	0.69	8.33e+10
NGC4930	Bulge+Disk+Bar	SB(rs)b	B	36.73	-20.84	0.90	1.61e+11
NGC4939	PSF+Bulge+Disk	SA(s)bc	A	44.16	-21.34	0.64	1.43e+11
NGC4941	PSF+Bulge+Disk	(R)SAB(r)ab	AB	12.09	-18.52	0.84	2.50e+10
NGC4941	PSF+Bulge+Disk	(R)SAB(r)ab	AB	12.09	-18.52	0.84	2.50e+10
NGC4995	PSF+Bulge+Disk+Bar	SAB(rs)b	AB	24.90	-20.39	0.87	8.25e+10
NGC5054	Bulge+Disk	SA(s)bc	A	25.59	-20.38	0.76	8.31e+10
NGC5085	Bulge+Disk	SA(s)c	A	27.96	-20.67	0.87	2.54e+10
NGC5101	Bulge+Disk+Bar	(R)SB(rs)0	B	26.28	-20.48	1.00	1.69e+11
NGC5121	PSF+Bulge+Disk	(R')SA(s)a	A	21.46	-20.16	0.95	3.68e+10
NGC5161	Bulge+Disk+Bar	SA(s)c	A	34.32	-20.69	0.79	1.65e+11
NGC5247	Bulge+Disk	SA(s)bc	A	19.51	-20.96	0.54	3.86e+10
NGC5371	Bulge+Disk+Bar	SAB(rs)bc	AB	36.78	-21.52	0.70	1.74e+11
NGC5427	Bulge+Disk	SA(s);pec	A	19.51	-20.97	0.57	4.61e+10
NGC5483	Bulge+Disk+Bar	SA(s)c	A	25.32	-	-	-
NGC5643	PSF+Bulge+Disk+Bar	SAB(rs)c	AB	16.62	-20.37	0.74	6.68e+10
NGC5676	Bulge+Disk	SA(rs)bc	A	30.59	-20.57	0.68	9.01e+10
NGC5701	PSF+Bulge+Disk+Bar	(R)SB(rs)0	B	22.23	-19.98	0.88	4.67e+10
NGC5713	Bulge+Disk	SAB(rs)bc;pec	AB	26.90	-20.32	0.64	5.21e+10
NGC5850	Bulge+Disk+Bar	SB(r)b	B	35.47	-21.22	0.79	1.37e+11
NGC5921	PSF+Bulge+Disk+Bar	SB(r)bc	B	20.82	-20.11	0.66	3.51e+10
NGC5962	Bulge+Disk+Bar	SA(r)c	A	28.47	-20.30	0.64	4.43e+10
NGC6215	Bulge+Disk	SA(s)c	A	21.73	-19.69	0.54	1.84e+10
NGC6221	Bulge+Disk+Bar	SB(s)bc;pec	B	19.29	-20.77	0.74	1.31e+11
NGC6300	Bulge+Disk+Bar	SB(rs)b	B	15.85	-20.81	0.78	4.49e+10
NGC6384	Bulge+Disk	SAB(r)bc	AB	24.14	-20.78	0.72	1.05e+11
NGC6753	Bulge+Disk+Bar	(R)SA(r)b	A	44.88	-21.31	0.83	1.81e+11
NGC6782	Bulge+Disk+Bar	(R)SAB(r)a	AB	55.60	-	-	-
NGC6902	PSF+Bulge+Disk	SA(r)b	A	39.97	-21.44	0.71	8.12e+10
NGC6907	Bulge+Disk+Bar	SB(s)bc	B	44.64	-21.36	0.69	1.21e+11
NGC7083	Bulge+Disk	SA(s)bc	A	43.70	-21.35	0.65	1.05e+11
NGC7205	Bulge+Disk	SA(s)bc	A	21.17	-20.09	0.60	3.11e+10
NGC7213	PSF+Bulge+Disk	SA(s)a	A	25.76	-21.05	0.89	1.26e+11
NGC7217	PSF+Bulge+Disk	(R)SA(r)ab	A	13.36	-19.61	0.90	8.38e+10
NGC7412	Bulge+Disk+Bar	SB(s)b	B	24.51	-20.07	0.53	1.50e+10
NGC7479	PSF+Bulge+Disk+Bar	SB(s)c	B	34.20	-21.08	0.75	1.44e+11
NGC7552	Bulge+Disk+Bar	(R')SB(s)ab	B	23.61	-20.62	0.68	3.49e+10
NGC7723	Bulge+Disk+Bar	SB(r)b	B	27.07	-20.23	0.73	4.32e+10
NGC7727	Bulge+Disk	SAB(s)a;pec	AB	26.23	-20.60	0.91	1.13e+11
NGC7741	Bulge+Disk+Bar	SB(s)cd	B	10.79	-18.33	0.53	6.67e+09
NGC7814	Bulge+Disk	SA(s)ab;sp	AB	14.88	-19.31	0.99	8.02e+10

Note. — Columns are : (1) Galaxy name. (2) The best fit chosen based on the criteria outlined in §3.3. (3) Hubble type from RC3 (de Vaucouleurs et al. 1991). (4) RC3 bar type, which is based on visual inspection of optical images and runs as ‘B’=‘strongly barred’, ‘AB’=‘weakly barred’, and ‘A’=‘unbarred’. (5) Distance in Mpc calculated assuming a Hubble constant of 70 km s<sup>-1</sup> Mpc<sup>-1</sup>. (6) Extinction and k-corrected absolute B-band magnitude from Hyperleda. (7)  $B - V$  color from Hyperleda. (8) Stellar mass, calculated as outlined in §2.2.

Table 2. Decomposition For NGC 4643

Fit		$r_e$ or h ( $''$ )	$r_e$ or h (kpc)	$n$	$b/a$	Position Angle	Fractional light
Stage 1	Sérsic	27.90	2.66	4.44	0.80	-51.03	100%
Stage 2	Bulge	23.86	2.30	4.16	0.80	-51.08	34.6%
	Disk	335.88	32.33	1.00	0.84	66.94	65.4%
Stage 3	Bulge	5.43	0.52	2.53	0.90	60.52	25.0%
	Disk	48.22	4.64	1.00	0.84	66.94	54.1%
	Bar	21.30	2.05	0.62	0.37	-45.84	20.9%

Table 3. Decomposition For NGC 4548

Fit		$r_e$ or h ( $''$ )	$r_e$ or h (kpc)	$n$	$b/a$	Position Angle	Fractional light
Stage 1	Sérsic	154.59	5.19	5.19	0.80	78.31	100%
Stage 2	Bulge	57.86	1.94	4.32	0.76	75.77	61.5%
	Disk	60.39	2.03	1.00	0.75	-32.54	38.5%
Stage 3	Bulge	6.98	0.23	1.56	0.88	-66.50	13.0%
	Disk	58.22	1.96	1.00	0.75	-32.54	68.6%
	Bar	44.91	1.51	0.51	0.35	66.65	18.4%

Table 4. Decomposition For NGC 4902

Fit		$r_e$ or h ( $''$ )	$r_e$ or h (kpc)	$n$	$b/a$	Position Angle	Fractional light
Stage 1	Sérsic	284.2	53.0	6.48	0.54	69.1	100%
Stage 2	Bulge	20.1	3.75	3.12	0.45	69.1	31.2%
	Disk	24.4	6.42	1.00	0.84	81.1	68.8%
Stage 3	Bulge	3.60	0.67	2.58	2.58	64.4	6.24%
	Disk	30.5	5.69	1.00	0.84	81.1	83.8%
	Bar	14.1	2.63	0.37	0.37	9.98	9.98%

Table 5. Checking GALFIT robustness with different input guesses for Stage 3

	$B/T$	Bulge $r_e$ ( $''$ )	Bulge $n$	$D/T$	Disk $h$ ( $''$ )	Bar/ $T$	Bar $r_e$ ( $''$ )	Bar $n$
<b>NGC 4548</b>								
Initial guesses from 1D decomposition	17.5%	7.39	1.17	63.5%	28.4	19.0%	37.5	0.54
Stage 3 Output	13.0%	6.98	1.56	68.6%	58.2	18.4%	44.9	0.51
Initial guesses from Stage 2	11.1%	7.50	1.70	69.9%	64.5	19.1%	37.5	0.54
Stage 3 Output	13.0%	6.98	1.56	68.6%	58.2	18.4%	44.9	0.51
<b>NGC 4643</b>								
Initial guesses from 1D decomposition	33.6%	7.18	0.86	40.4%	37.5	26.0%	22.0	0.60
Stage 3 Output	25.0%	5.43	2.53	54.1%	48.2	20.9%	21.3	0.62
Initial guesses from Stage 2	24.1%	5.30	2.5	51.8%	46.4	24.1%	22.0	0.60
Stage 3 Output	25.0%	5.43	2.53	54.1%	48.2	20.9%	21.3	0.62

Table 6. Mass Breakdown of Galactic Structures

Structure	Mass
Bulges	$20.2\% \pm 3.55\%$
Disks	$69.9\% \pm 4.06\%$
Bars	$9.92\% \pm 2.64\%$
Bulges with $n > 2$	$15.5\% \pm 3.20\%$
Bulges with $n \leq 2$	$4.74\% \pm 1.88\%$

Table 7.  $B/T$  and bulge  $n$  in bright/high mass spirals

Sample ( $M_B < -19.3$ )	
Fraction of spirals with bulge $n \geq 4$	$4.79\% \pm 1.77\%$
Fraction of spirals with bulge $2 < n < 4$	$35.6\% \pm 3.96\%$
Fraction of spirals with bulge $n \leq 2$	$59.6\% \pm 4.06\%$
Fraction of spirals with bulge $n > 2$	$40.4\% \pm 4.06\%$
Fraction of spirals with $B/T \leq 0.2$	$69.2\% \pm 3.82\%$
Fraction of spirals with $B/T > 0.2$	$30.8\% \pm 3.82\%$
Fraction of spirals with $0.2 < B/T < 0.4$	$21.9\% \pm 3.42\%$
Fraction of spirals with $B/T \geq 0.4$	$8.90\% \pm 2.36\%$
Sample $M_\star \geq 1 \times 10^{10} M_\odot$	
Fraction of spirals with bulge $n \geq 4$	$6.19\% \pm 2.27\%$
Fraction of spirals with bulge $2 < n < 4$	$37.2\% \pm 4.54\%$
Fraction of spirals with bulge $n \leq 2$	$56.6\% \pm 4.66\%$
Fraction of spirals with bulge $n > 2$	$4.34\% \pm 4.66\%$
Fraction of spirals with $B/T \leq 0.2$	$66.4\% \pm 4.44\%$
Fraction of spirals with $B/T > 0.2$	$33.6\% \pm 4.44\%$
Fraction of spirals with $0.2 < B/T < 0.4$	$23.0\% \pm 3.96\%$
Fraction of spirals with $B/T \geq 0.4$	$10.6\% \pm 2.90\%$

Table 8. Bar Fraction as a Function of  $B/T$  and Bulge Index

Sample ( $M_B < -19.3$ )	
Bar fraction in spirals with bulge $n \geq 4$	$28.6\% \pm 17.1\%$
Bar fraction in spirals with bulge $2 < n < 4$	$51.9\% \pm 6.93\%$
Bar fraction in spirals with bulge $n \leq 2$	$64.4\% \pm 5.13\%$
Bar fraction of spirals with bulge $n > 2$	$49.2\% \pm 6.51\%$
Bar fraction of spirals with $B/T \leq 0.2$	$68.3\% \pm 4.63\%$
Bar fraction of spirals with $B/T > 0.2$	$35.6\% \pm 7.14\%$
Bar fraction of spirals with $0.2 < B/T < 0.4$	$37.5\% \pm 8.56\%$
Bar fraction of spirals with $B/T \geq 0.4$	$30.8\% \pm 12.8\%$
Sample $M_\star \geq 1 \times 10^{10} M_\odot$	
Bar fraction of spirals with bulge $n \geq 4$	$28.6\% \pm 17.1\%$
Bar fraction of spirals with bulge $2 < n < 4$	$52.4\% \pm 7.71\%$
Bar fraction of spirals with bulge $n \leq 2$	$64.1\% \pm 6.00\%$
Bar fraction of spirals with bulge $n > 2$	$49.0\% \pm 7.14\%$
Bar fraction of spirals with $B/T \leq 0.2$	$68.0\% \pm 5.39\%$
Bar fraction of spirals with $B/T > 0.2$	$36.8\% \pm 7.83\%$
Bar fraction of spirals with $0.2 < B/T < 0.4$	$38.5\% \pm 9.54\%$
Bar fraction of spirals with $B/T \geq 0.4$	$33.3\% \pm 13.6\%$

Table 9.  $B/T$  : Data versus Hierarchical Models of Galaxy Evolution

	Data	Model (Major+Minor)	Model (Minor Only)	Model (Minor Only + (Minor+Major) )
Fraction of spirals with $B/T \leq 0.2$	$66.4\% \pm 4.44\%$	3.09%	64.1%	67.19%
Fraction of spirals with $0.2 < B/T \leq 0.4$	$23.0\% \pm 3.95\%$	5.80%	13.1%	18.90%
Fraction of spirals with $0.4 < B/T \leq 0.6$	$7.96\% \pm 2.54\%$	6.76%	1.15%	7.91%
Fraction of spirals with $0.6 < B/T \leq 0.75$	$2.65\% \pm 1.51\%$	6.02%	0.03%	6.05%

Table 10. Comparison of model merger fraction and bulge Sérsic index distribution

Stellar mass limit: $1.0 \times 10^{10} M_{\odot}$	
Model galaxies: 7641	
Observed galaxies: 113	
<b>Test 1</b>	
% of model galaxies w/ $B/T \leq 0.2$ with no past major merger	$4897/7641 = 64.09\% \pm 0.55\%$
% of observed galaxies w/ $B/T \leq 0.2$ and bulge $n \leq 3$ :	$71/113 = 62.83\% \pm 4.55\%$
% of observed galaxies w/ $B/T \leq 0.2$ and bulge $n \leq 2.5$ :	$65/113 = 57.5\% \pm 4.65\%$
% of observed galaxies w/ $B/T \leq 0.2$ and bulge $n \leq 2$ :	$53/113 = 46.90\% \pm 4.69\%$
<b>Test 2</b>	
% of model galaxies w/ $B/T \geq 0.4$ and a past major merger:	$974/7641 = 12.75\% \pm 0.38\%$
% of observed spirals w/ $B/T \geq 0.4$ and bulge $n > 3$ :	$6/113 = 5.31\% \pm 2.10\%$
% of observed spirals w/ $B/T \geq 0.4$ and bulge $n > 2.5$ :	$8/113 = 7.08\% \pm 2.41\%$
% of observed spirals w/ $B/T \geq 0.4$ and bulge $n > 2$ :	$10/113 = 8.65\% \pm 2.67\%$
<b>Test 3</b>	
% of model galaxies w/ $B/T \leq 0.2$ and a past major merger:	$236/7641 = 3.09\% \pm 0.20\%$
% of observed galaxies w/ $B/T \leq 0.2$ and bulge $n > 3$ :	$4/113 = 3.54\% \pm 1.74\%$
% of observed galaxies w/ $B/T \leq 0.2$ and bulge $n > 2.5$	$10/113 = 8.85\% \pm 2.67\%$
% of observed galaxies w/ $B/T \leq 0.2$ and bulge $n > 2$	$22/113 = 19.47\% \pm 3.72\%$

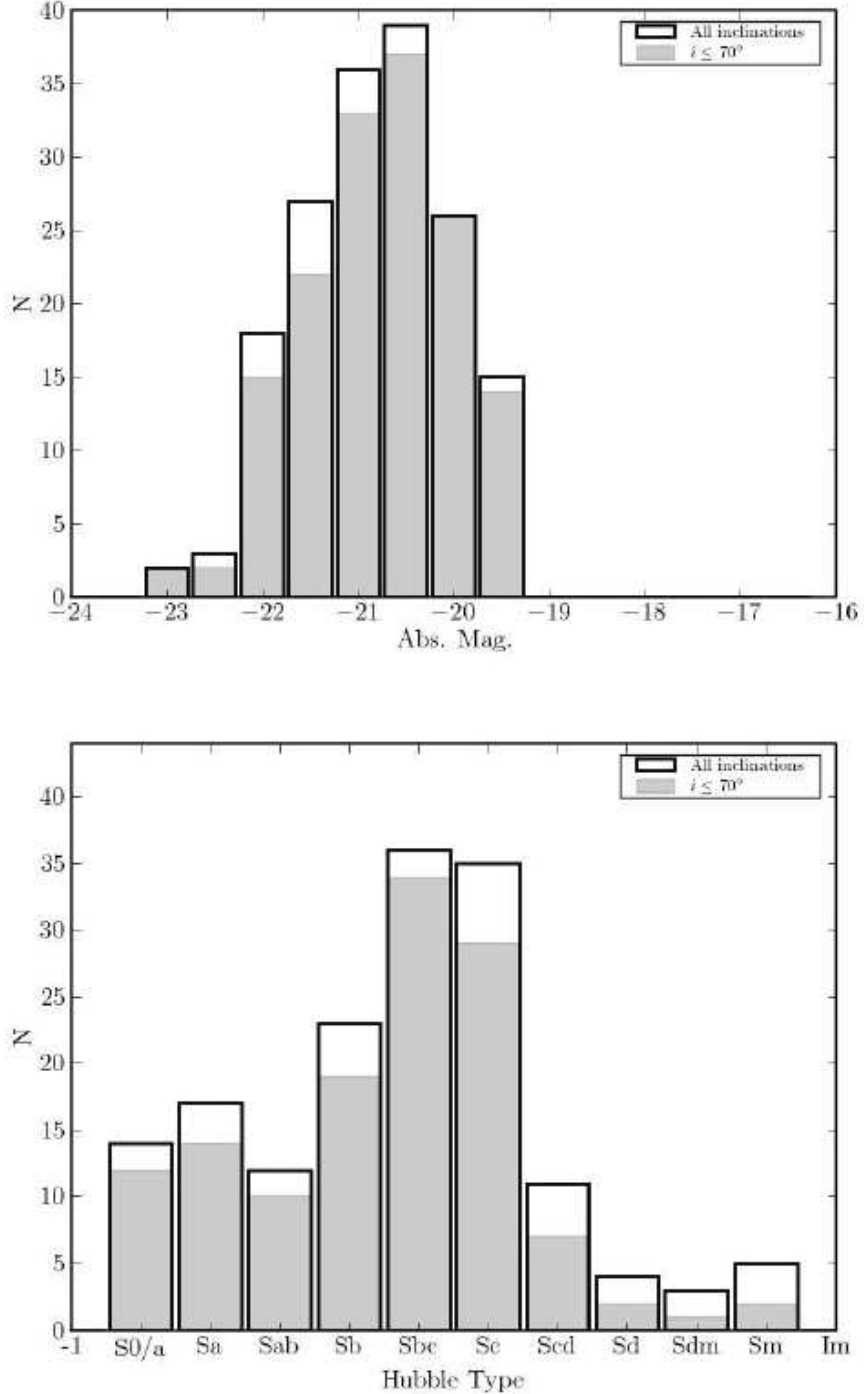


Fig. 1.— Our final sample S1 consists of 146 bright ( $M_B < -19.3$ ) moderately inclined ( $i \leq 70^\circ$ ) spirals in the OSUBSGS survey. The distribution of absolute  $B$ -band magnitude for the sample of bright spirals in the OSUBSGS survey is shown in the top panel before (solid line) and after (shaded greyscale) the cut to remove highly inclined ( $i > 70^\circ$ ) spirals. The distribution of Hubble types for the sample is shown in the bottom panel before (solid line) and after (shaded greyscale) the cut to remove highly inclined ( $i > 70^\circ$ ) spirals.

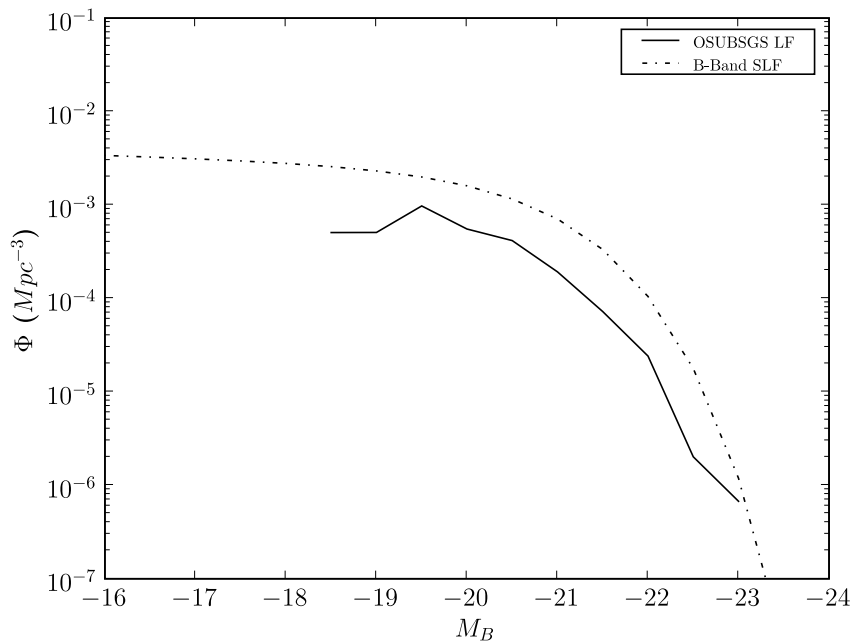


Fig. 2.— The luminosity function of the full OSUBSGS sample is compared to the *B*-band Schechter luminosity function (SLF). The former is calculated as described in §2.1 using equation (1). The parameters for the SLF are  $\Phi^* = 5.488 \times 10^{-3} \text{ Mpc}^{-3}$ ,  $\alpha = -1.07$ , and  $M_B^* = -20.5$  (Efstathiou, Ellis & Peterson 1988), corresponding to  $H_0 = 70 \text{ km/s Mpc}^{-1}$ .

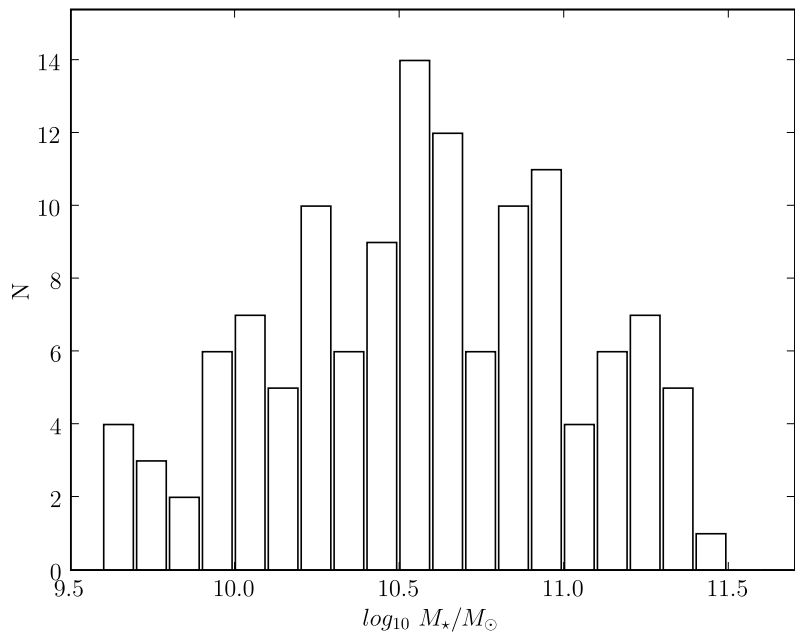


Fig. 3.— Out of our final sample S1 of 146 bright ( $M_B < -19.3$ ) moderately inclined ( $i \leq 70^\circ$ ) OSUBSGS spirals, stellar masses could be estimated for 127 galaxies. Their stellar mass distribution is shown, as determined in § 2.2. Most have stellar masses  $M_* \geq 1.0 \times 10^{10} M_\odot$ . This sample of 127 galaxies is referenced henceforth as the sample S2.

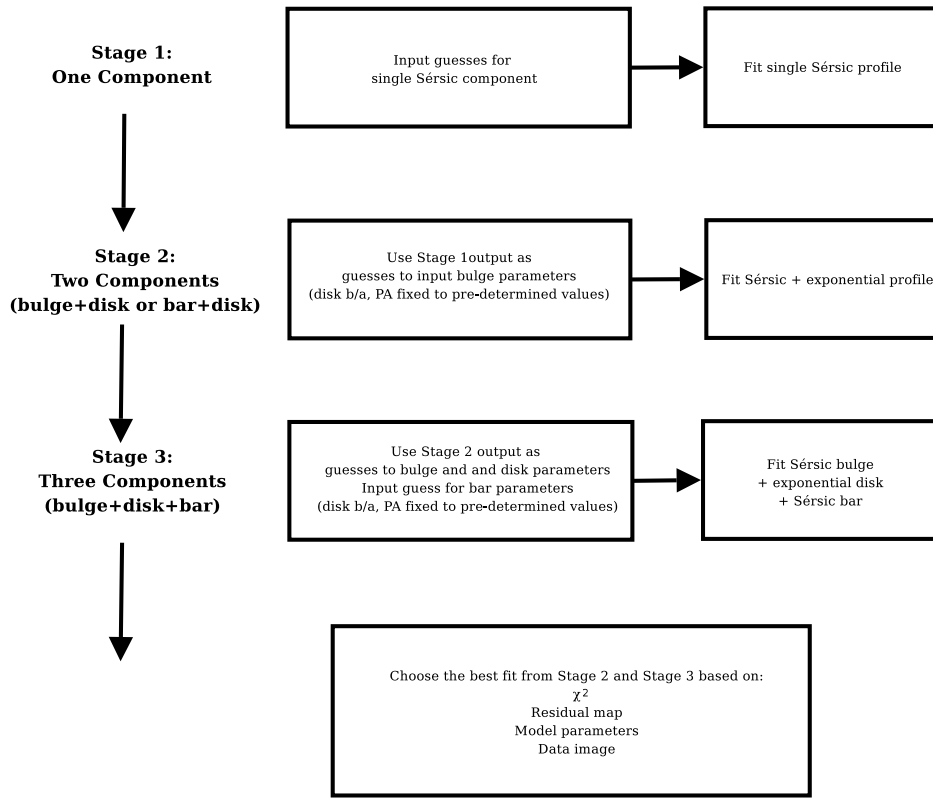


Fig. 4.— An overview of the method of decomposition. All images are subjected to Stages 1, 2, and 3. Either the best fit of Stage 2 or Stage 3 is chosen as the best model.

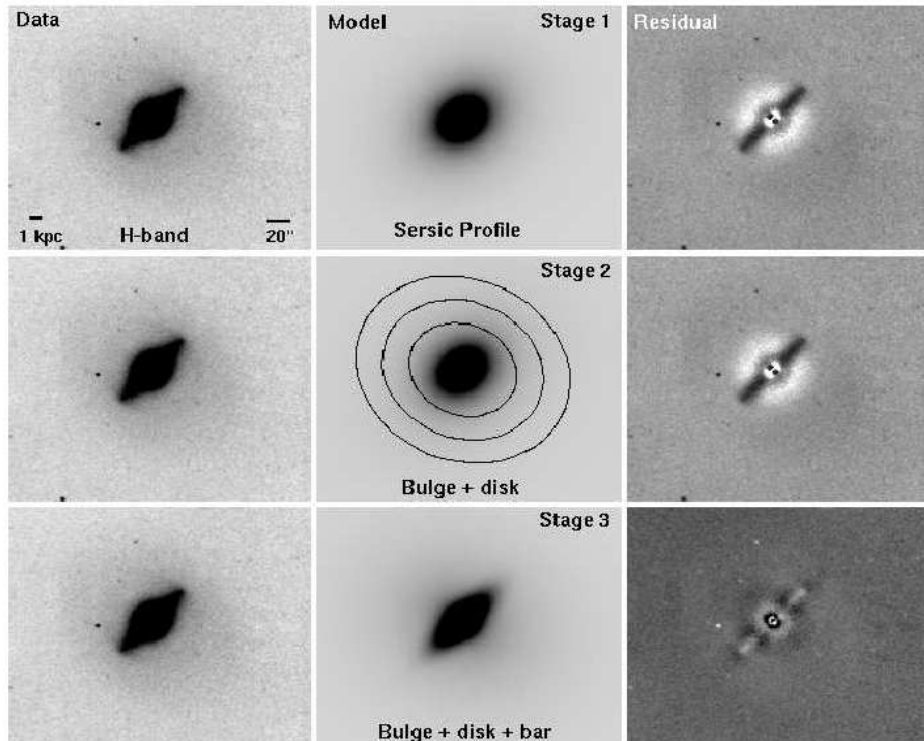


Fig. 5.— Complete 2D decomposition for NGC 4643. Note the prominent bar residuals in the residual for the Stage 1 and Stage 2 bulge-disk decomposition. This is a case where the prominent bar causes the Stage 2 bulge-disk fit to artificially extend the bulge and inflate the  $B/T$ . The disk fitted in Stage 2 has a low surface brightness and is very extended, well beyond the real disk: the  $b/a$  and  $PA$  of the fitted disk is shown as contours. Stage 3 bulge-disk-bar decomposition provides the best model. See Table 2 for the fit parameters.

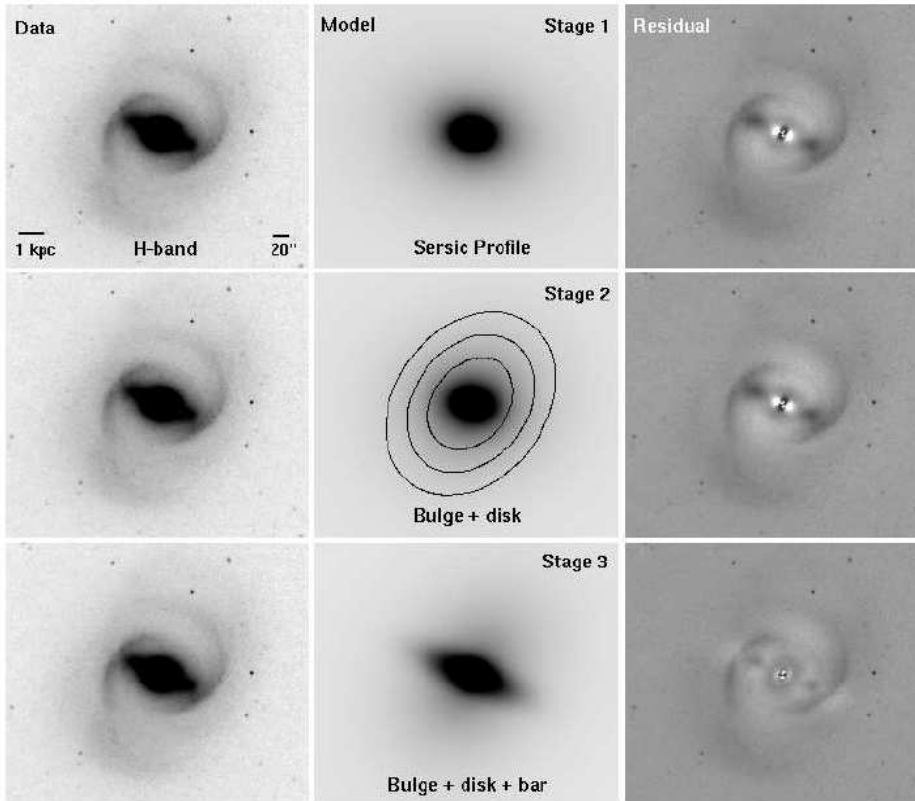


Fig. 6.— The complete 2D decomposition for NGC 4548. This is an extreme example where the prominent bar results in an extended bulge and inflated  $B/T$  in the Stage 2 bulge-disk fit. Like NGC 4643 in Figure 5, the disk fitted in Stage 2 has a low surface brightness and is very extended: its  $b/a$  and  $PA$  are shown as contours. Stage 3 bulge-disk-bar decomposition provides the best model. See Table 3 for the fit parameters.

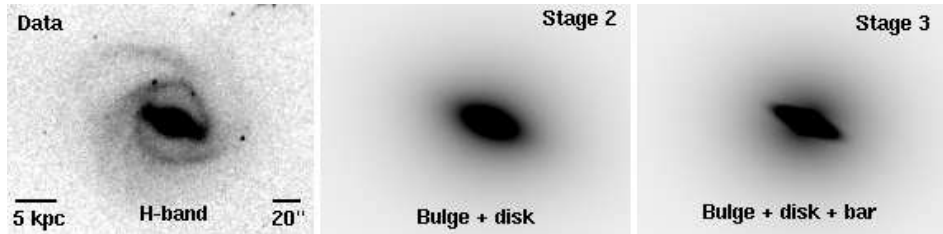


Fig. 7.— This plot shows the data image, Stage 2 model, and Stage 3 model for NGC 4902. The Stage 2 bulge is too bright and is extended along the major axis of the bar ( $B/T=31.2\%$  and  $b/a=0.45$ ). In Stage 3, the bulge and bar are fit with distinct components ( $B/T=6.2\%$ , bulge  $b/a=0.75$ , Bar/ $T=10.0\%$ , bar  $b/a=0.25$ ). All other fit parameters appear in Table 4.

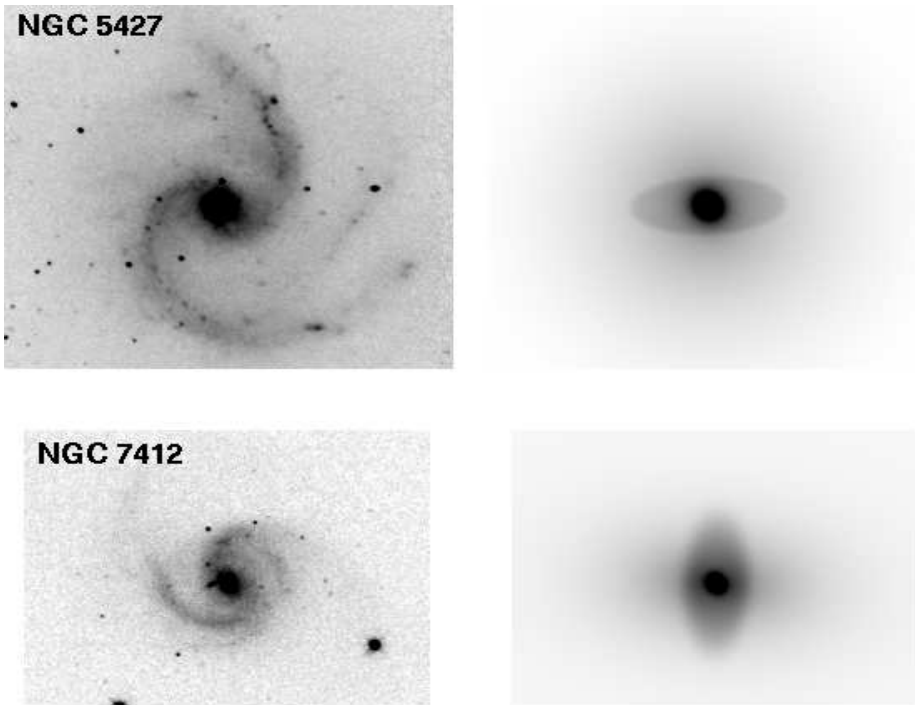


Fig. 8.— The data images and Stage 3 bulge-disk-bar decomposition models of NGC 5427 and NGC 7412 are shown. The Stage 3 models each distinctly show a false bar component, which is not present in the data images. The false components can be inspired by prominent spiral arms, such as those present in these galaxies. Such cases are flagged during the visual inspection of fits and the Stage 3 bulge-disk-bar decomposition is discarded in favor of the Stage 2 bulge-disk decomposition.

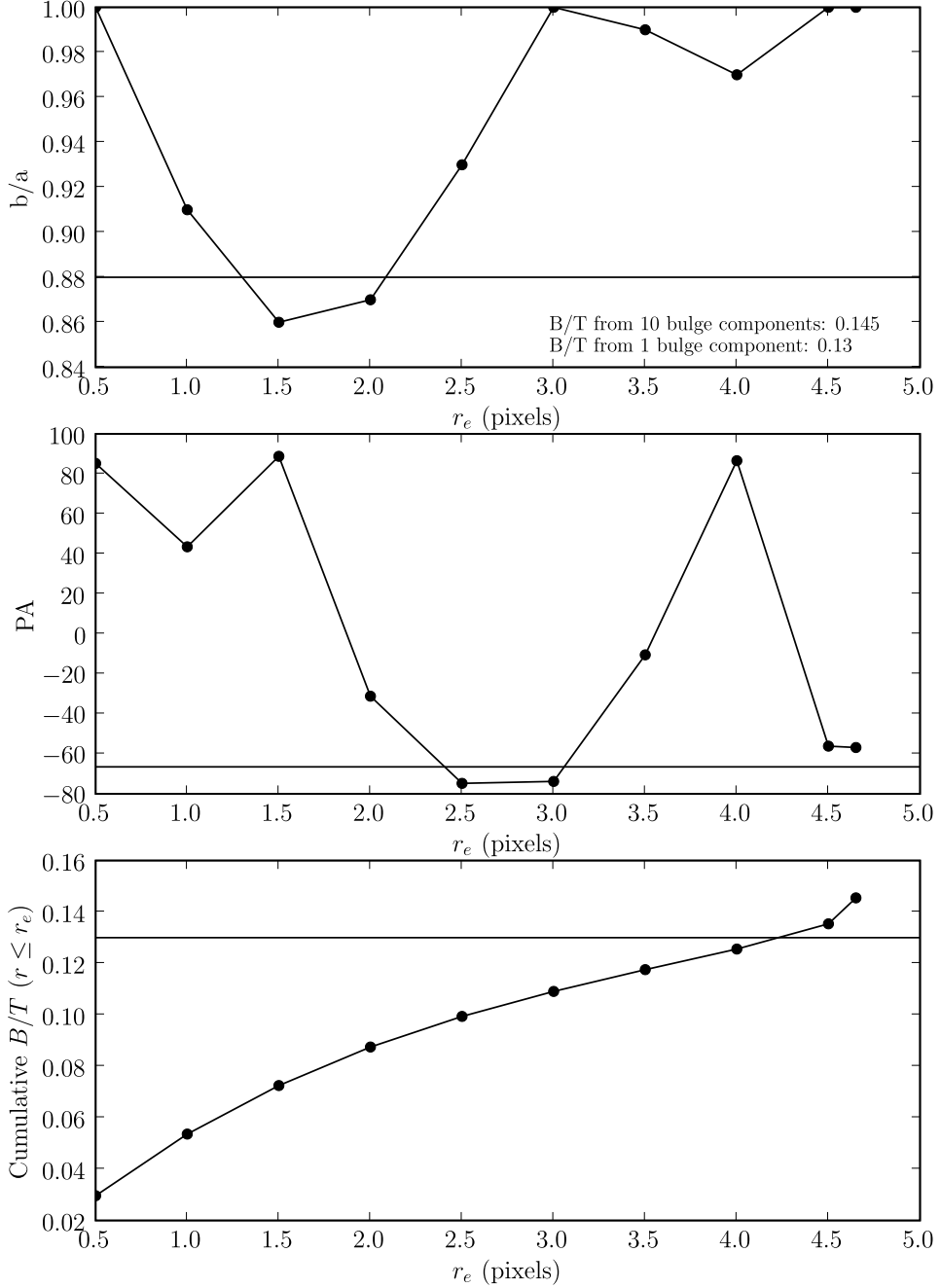


Fig. 9.— This plot compares the  $B/T$  obtained by fitting the bulge of NGC 4548 with a Sérsic model of constant  $b/a$  as opposed to a Sérsic model varying  $b/a$ . The bulge  $b/a$  (0.88),  $PA$  (-66.5), and  $B/T$  (13%) from the original Sérsic fit of constant  $b/a$  (Table 3) are indicated with horizontal lines on the 3 panels. To mimic the Sérsic model varying  $b/a$  in GALFIT, the bulge was fitted with ten concentric Sérsic profiles with fixed  $r_e$ , each separated by 0.75". The top two panels show the run of  $b/a$  and  $PA$  of the ten concentric Sérsic profiles. The bottom panel shows the cumulative  $B/T$  calculated by summing all models with  $r \leq r_e$ : the last point representing the summed  $B/T$  from all ten components is 14.5%, in good agreement with the 13.0% value from the Sérsic fit of constant  $b/a$ .

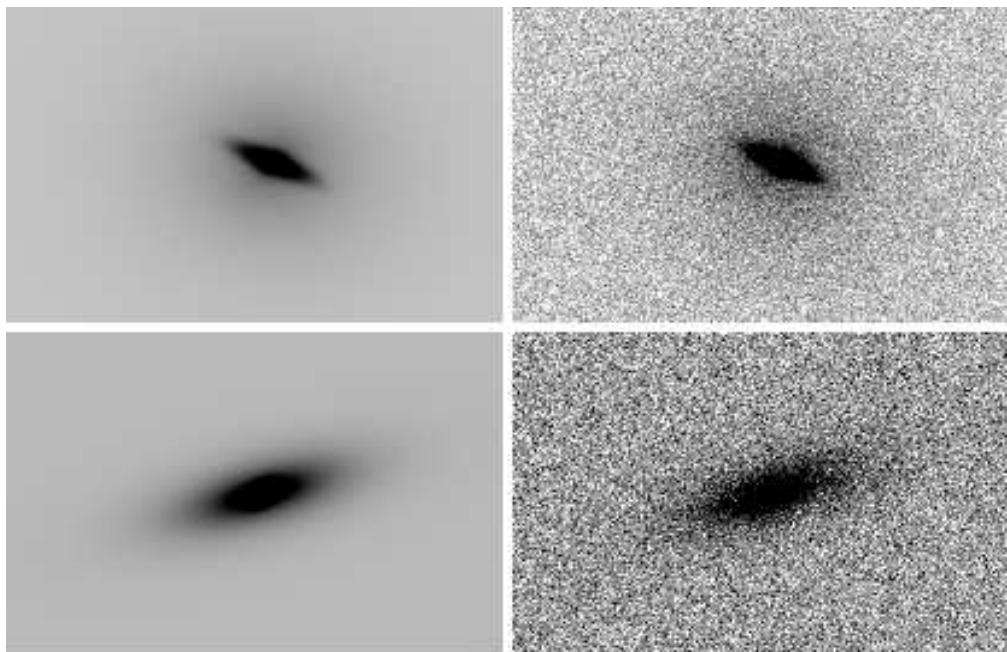


Fig. 10.— An elementary test is to determine if GALFIT can recover the known parameters of artificial noisy images. Noisy images were simulated by taking parametric model images (left panels) produced by GALFIT, and adding noise and sky background (right panels). The noisy images were then fitted to see if the original known parameters can be recovered. See §4.2 for details.

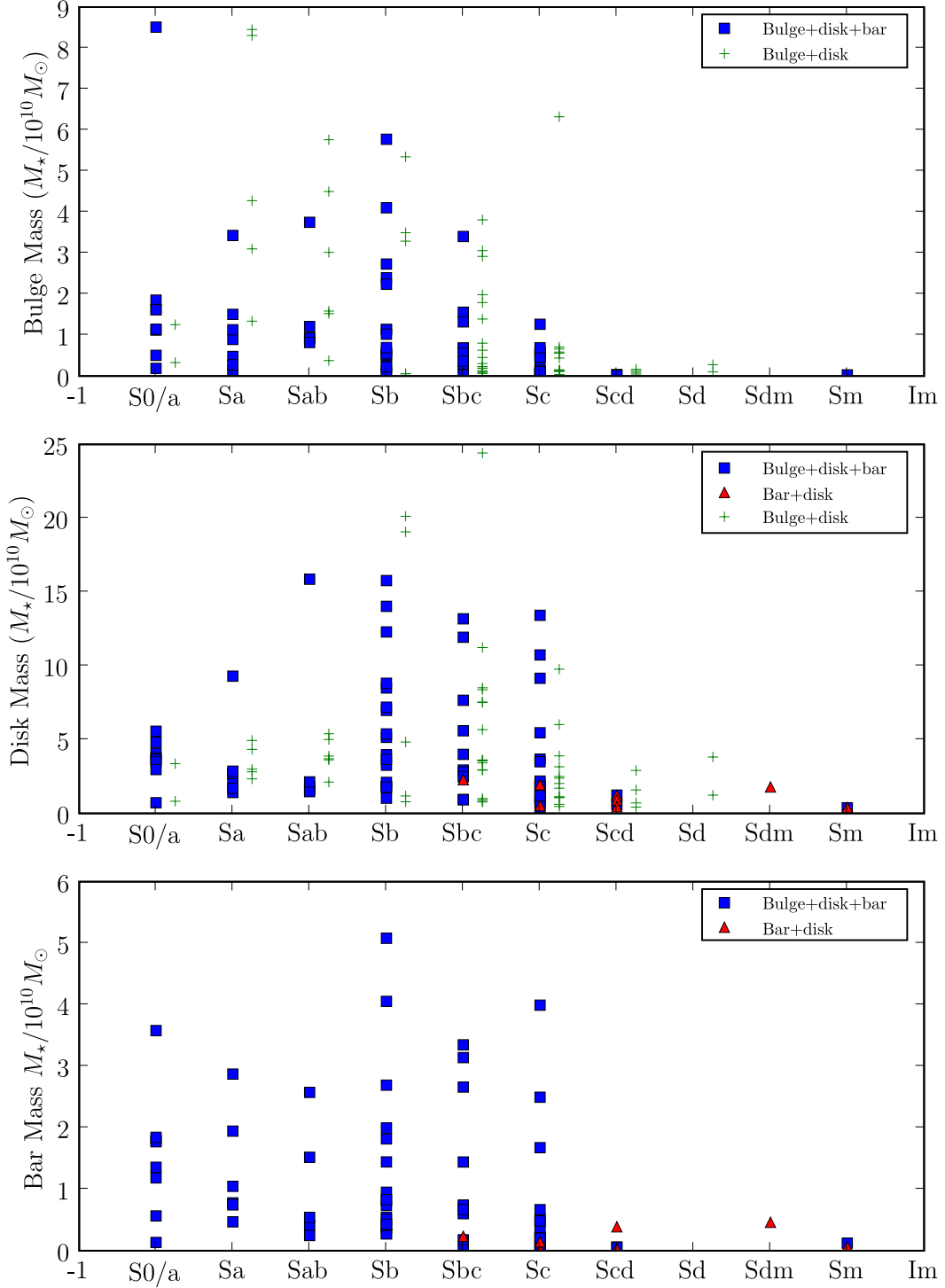


Fig. 11.— The top, middle, and bottom panels show stellar mass for bulges, disks, and bars, respectively, along the Hubble sequence. Values are shown for sample S2 of 127 galaxies in Fig. 3. The legend in each panel indicates the type of decomposition used for each data point.

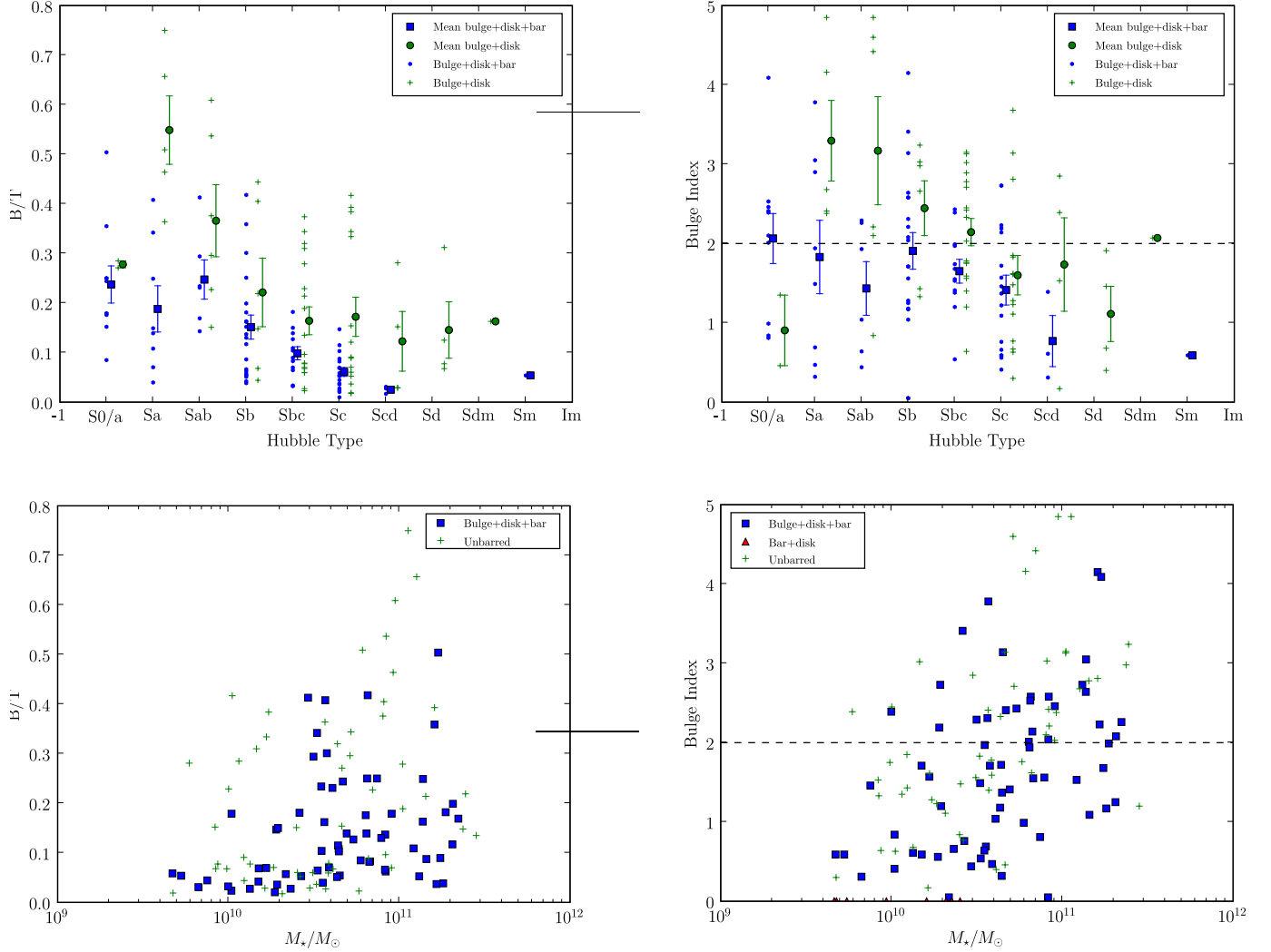


Fig. 12.— The legend in each panel indicates the type of decomposition used for each data point. The individual and mean  $B/T$  (left panels) and bulge Sérsic index (right panels) are plotted as a function of Hubble type for the sample S1 of bright galaxies, and as a function of galaxy stellar mass for sample S2. Barred and unbarred galaxies are shown separately. The error bars denote the error on the mean. The mean  $B/T$  and bulge index in barred galaxies differ systematically from unbarred galaxies, but there is a large overlap in the individual values. *As many as  $\sim 66\%$  of spiral galaxies have  $B/T \leq 0.2$ ; these bulges are pervasive and exist across the whole spectrum of S0/a to Scd.* Furthermore, *as many as  $59.6 \pm 4.06\%$  of bright spirals have low  $n \leq 2$  bulges: such bulges exist in barred and unbarred galaxies across all Hubble types, and their  $B/T$  ranges from 0.01 to 0.4, with most having  $B/T \leq 0.2$ .*

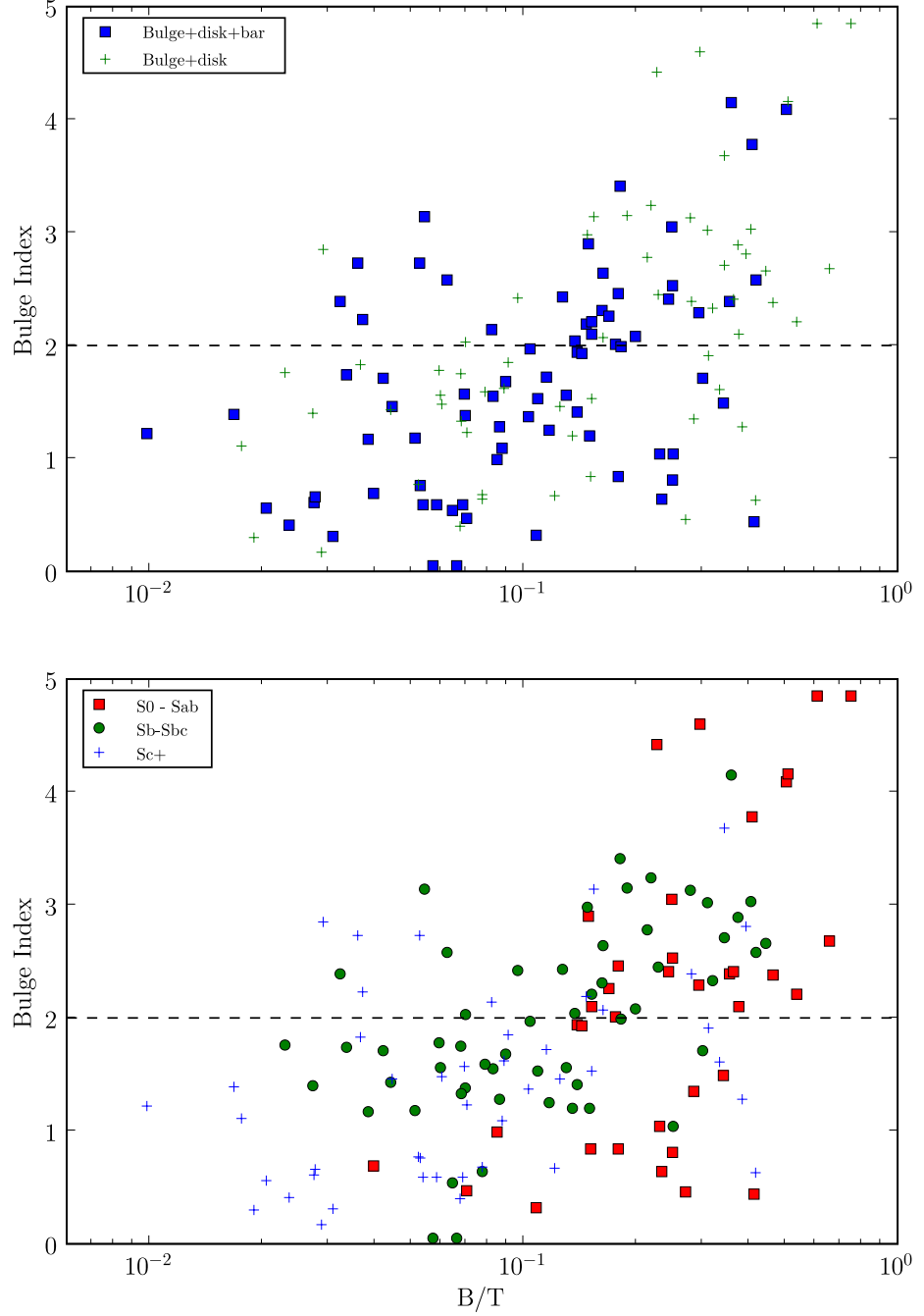


Fig. 13.— The relation between  $B/T$  and bulge index is shown. In the top panel, galaxies are coded according to bar class. The legend indicates the type of decomposition used for each data point. In the lower panel, galaxies are coded according to Hubble type. Only a small fraction ( $4.79\% \pm 1.77\%$ ) of bright spirals have high  $n \geq 4$  bulges: such bulges lie primarily in S0/a to Sab, and have a large  $B/T > 0.2$ . A moderate fraction ( $35.6\% \pm 3.96\%$ ) have intermediate  $2 < n < 4$  bulges: these exist in barred and unbarred S0/a to Sd, and their  $B/T$  spans a wide range (0.03 to 0.5) with a mean of 0.23. A striking  $59.6\% \pm 4.06\%$  of bright spirals have low  $n \leq 2$  bulges: such bulges exist in barred and unbarred galaxies across all Hubble types, and their  $B/T$  ranges from 0.01 to 0.4, with most having  $B/T \leq 0.2$ .

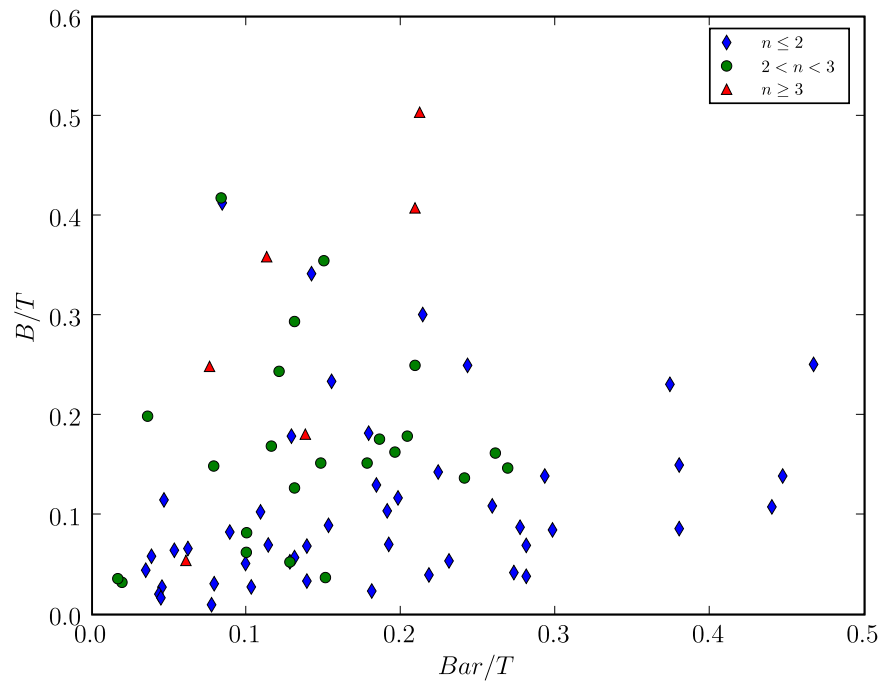


Fig. 14.—  $B/T$  is plotted against  $Bar/T$  and sorted by bulge Sérsic index. Aside from the six galaxies with large  $Bar/T$  ( $\geq 0.3$ ), most galaxies have moderate  $Bar/T$  and a wide range of  $B/T$  is seen at each  $Bar/T$ .

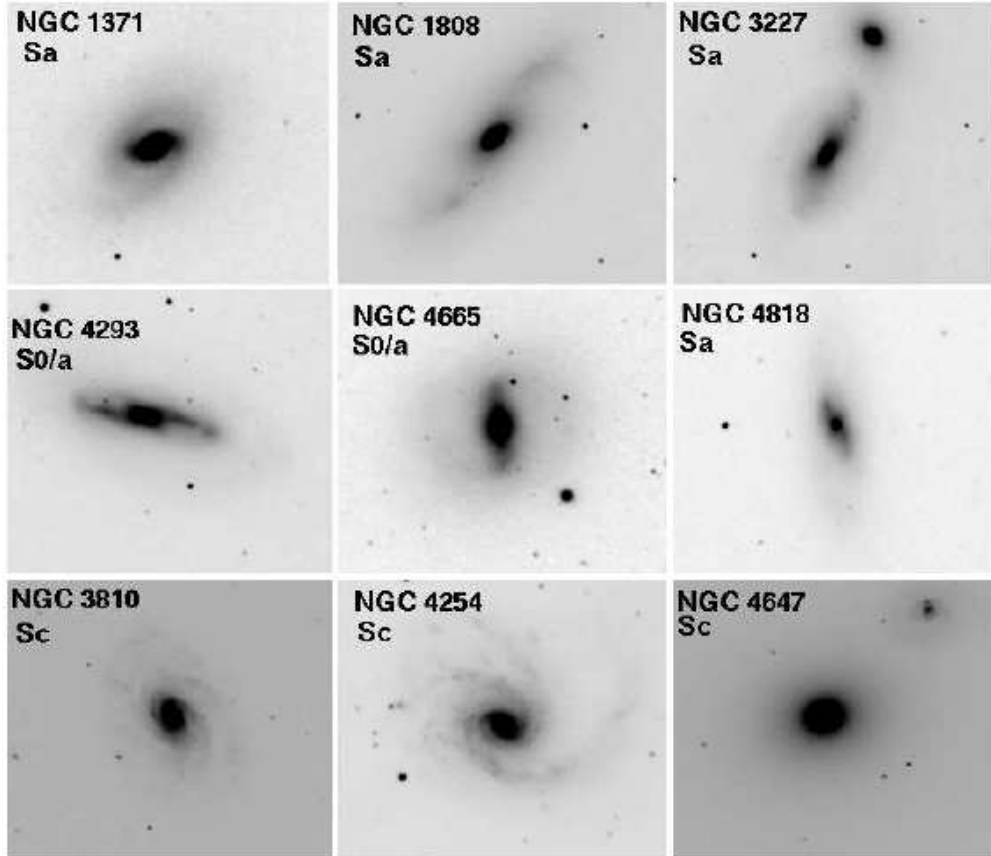


Fig. 15.— The **top two rows** shows barred galaxies, which have early RC3 Hubble types, but yet have  $B/T \leq 0.2$ . The images show that the bulge is not very conspicuous compared to the disk in most cases, and suggest that the measured low  $B/T$  values are in fact reasonable. Note that in the case of NGC 1371 and NGC 4665, there is an extended disk around a fairly prominent bulge. It is likely that these galaxies were assigned early Hubble types due to their smooth extended disks, although they have a low bulge-to-disk ratio. The **bottom row** shows unbarred galaxies, which have late RC3 Hubble types, but yet have  $B/T \sim 0.4$ . The images suggest that the large  $B/T$  are reasonable. In fact, NGC 4647 has such a prominent bulge and smooth disk that it is unclear why it was assigned a late RC3 Hubble type. The other two galaxies (NGC 3810 and NGC 4254) have prominent bulges and nuclear spiral arms. See § 5.3 for details.

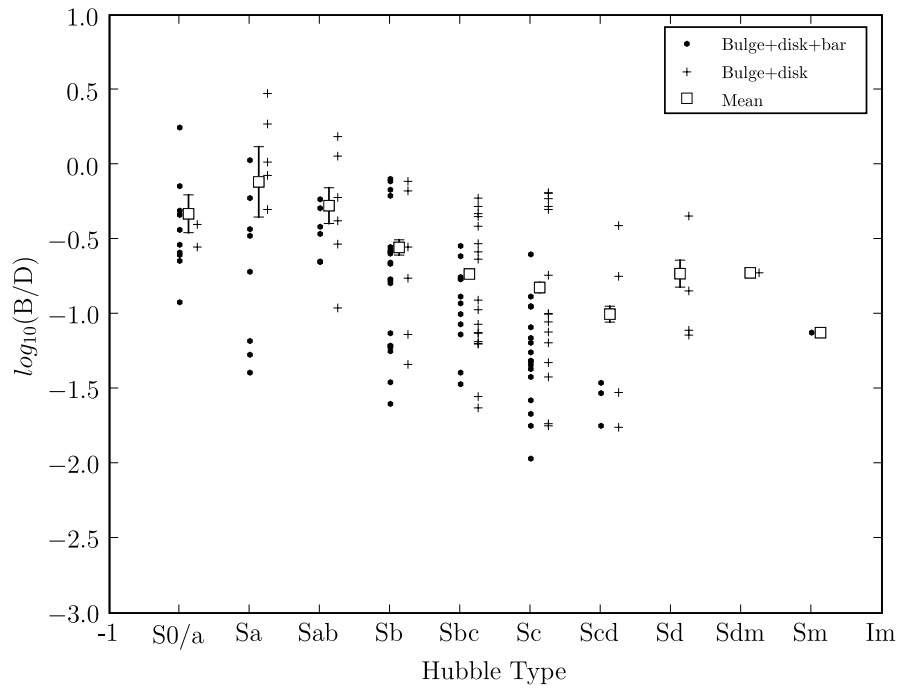


Fig. 16.— The legend indicates the type of decomposition used for each data point.  $B/D$  is plotted against Hubble type for our sample. Barred and unbarred populations are separated, but the mean values for barred and unbarred together in each bin are shown. This plot can be compared against the corresponding plot in Graham (2001), based on 1D fits of a smaller sample of galaxies. Our mean  $H$ -band  $B/D$  ratios are comparable to the mean  $K$ -band  $B/D$  in Graham (2001). Both studies also find that  $B/D$  shows a large range for each Hubble type, while the mean  $B/D$  declines from Sa to Sc galaxies.

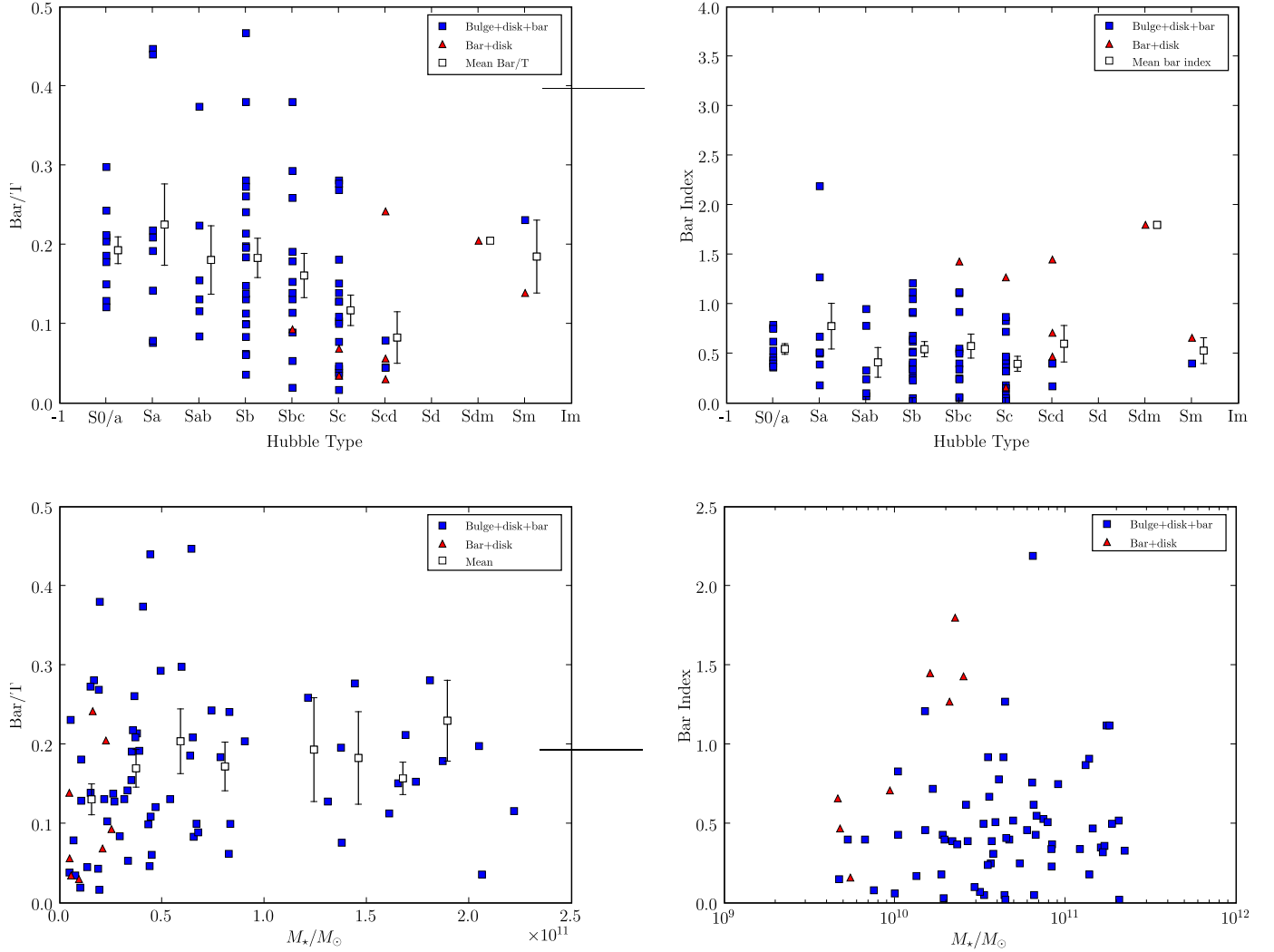


Fig. 17.— The properties of bars are shown. The legend in each panel indicates the type of decomposition used for each data point. Upper left: Mean and individual Bar/T plotted against Hubble type. Upper right: Mean and individual bar Sérsic indices plotted against Hubble type. Lower left: Bar/T plotted against total galaxy stellar mass. The mean Bar/T in bins of stellar mass is indicated. Lower right: Bar Sérsic index plotted against total galaxy stellar mass. All plots: the error bars where shown indicate error on the mean.

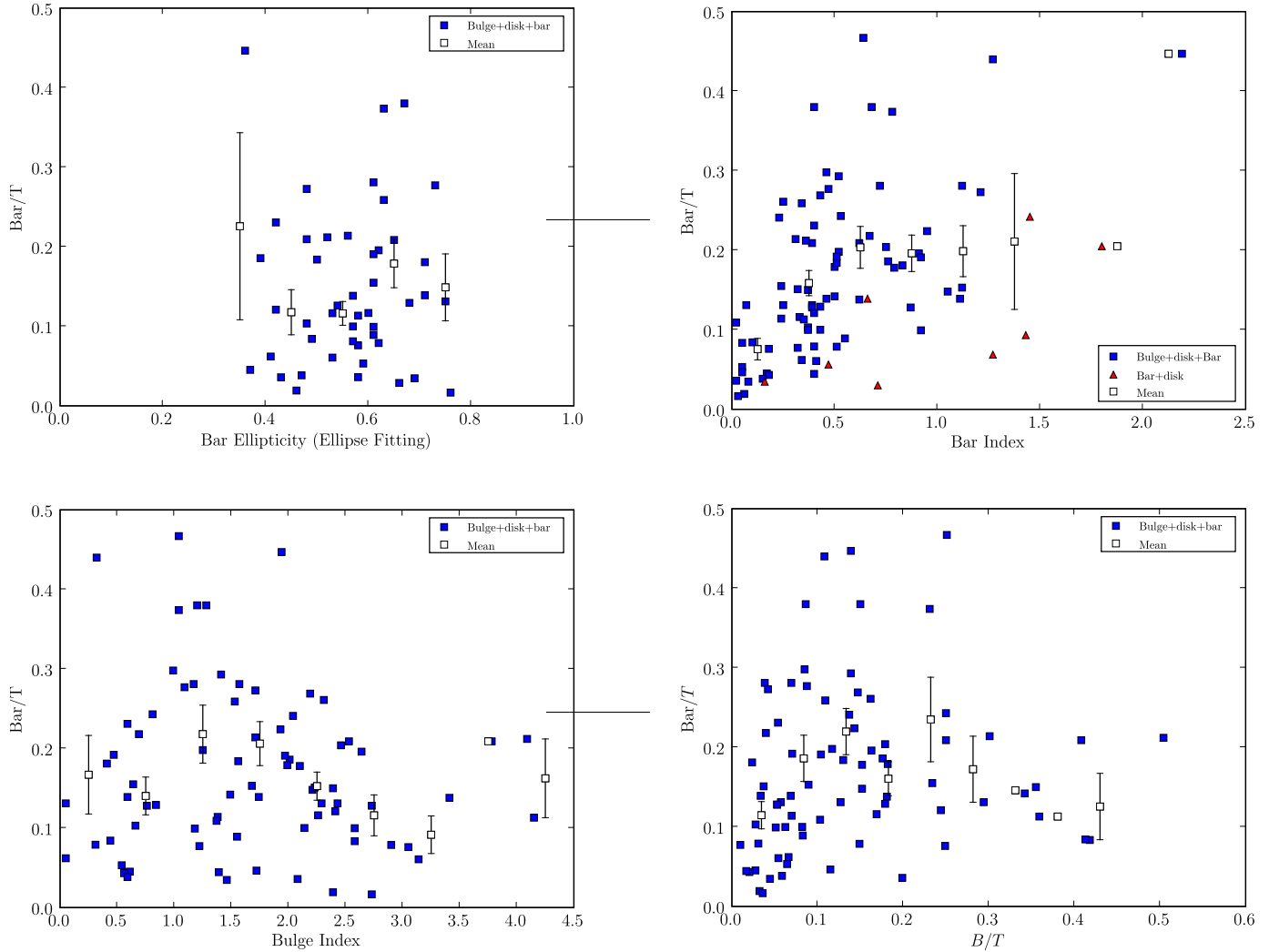


Fig. 18.— The legend in each panel indicates the type of decomposition used for each data point. The properties of bars are compared to bulges. Upper left:  $\text{Bar}/T$  is plotted against peak bar ellipticity from MJ07. Upper right:  $\text{Bar}/T$  is plotted against bar Sérsic index. Lower left:  $\text{Bar}/T$  is plotted against bulge Sérsic index. Lower right:  $\text{Bar}/T$  is plotted against  $B/T$ . All plots: mean  $\text{Bar}/T$  is calculated for bins along the ordinate axis, and the error bars indicate error on the mean.

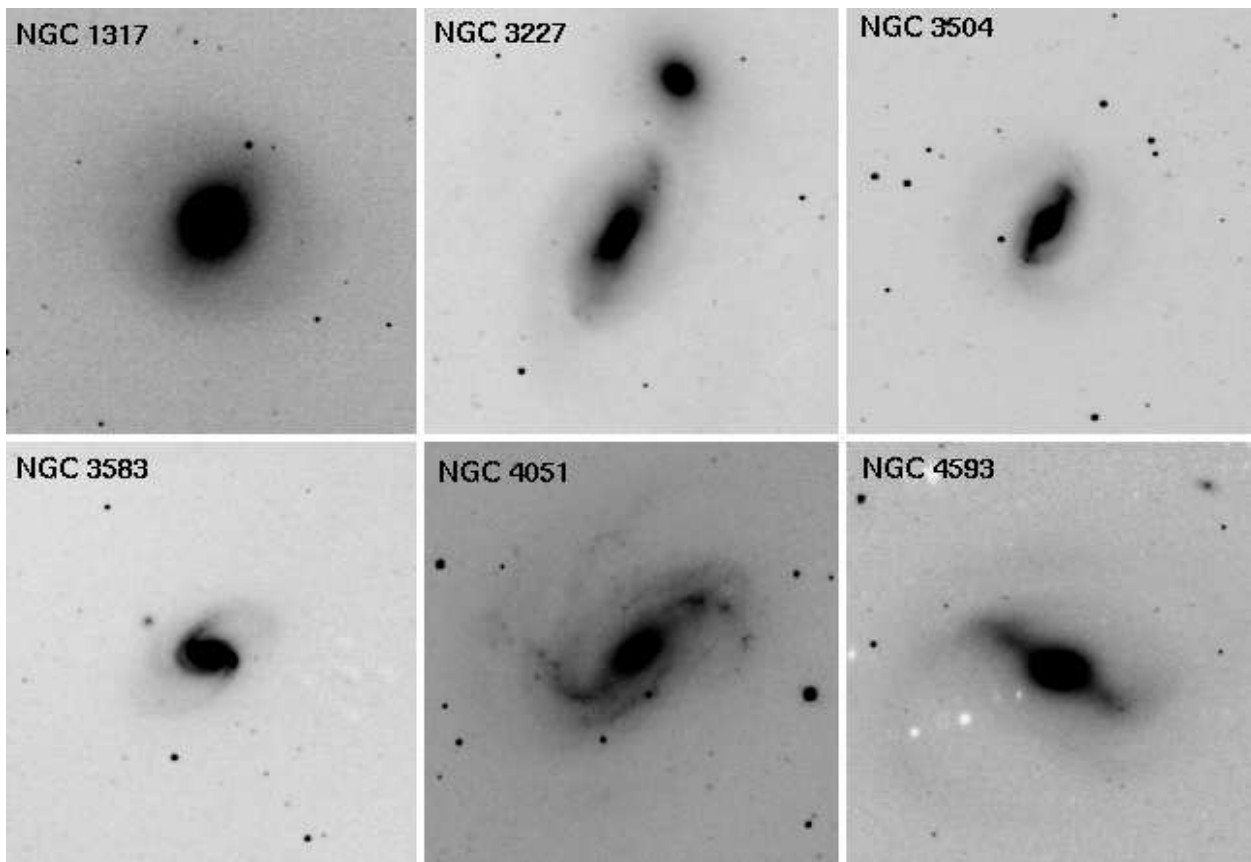


Fig. 19.—  $H$ -band images of spirals with large  $\text{Bar}/T$  ( $> 0.3$ ) are shown. The stellar bars are quite prominent in the images. An interesting example is the oval or lens galaxy NGC 1317: the bar has a low ellipticity, but its  $B/T$  is large because it is extended and massive. Such bars/lenses may exert significant gravitational torques although they are not very elongated.

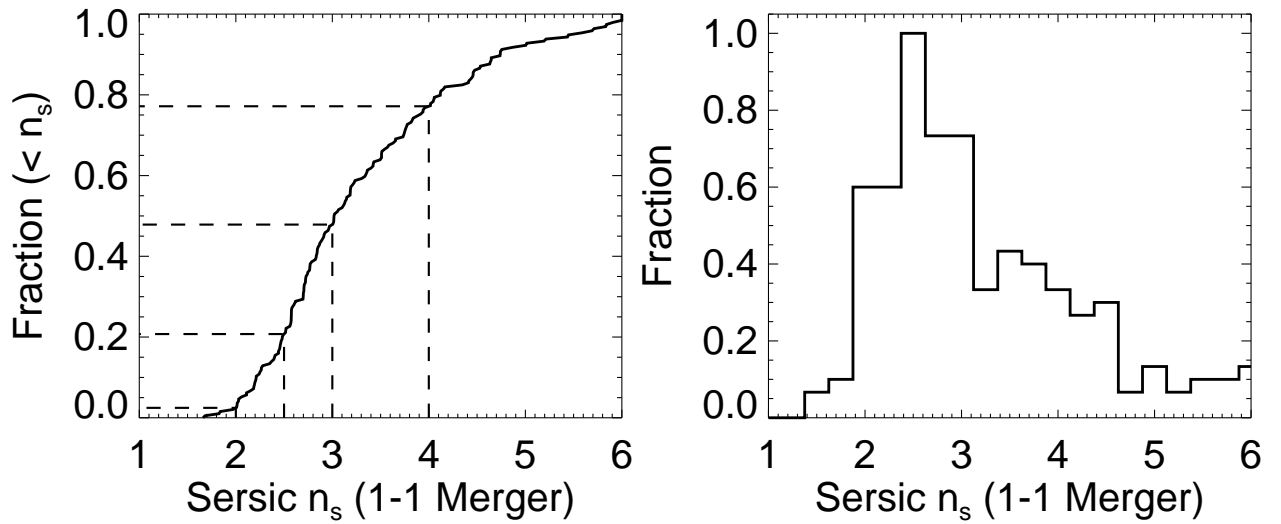


Fig. 20.— We show the distribution of Sérsic indices  $n$  for a representative set of 1:1 major merger remnants in the simulations of Hopkins et al. 2008 (in prep) : they lie in the range of  $2 < n < 4$ . Specifically,  $\sim 22\%$  of the remnants have classical  $n \geq 4$ , as much as 20% have low  $n \leq 2.5$ , while 50% have  $n \leq 3$ . Almost none have  $n \leq 2$ . [Figure: courtesy of Phil Hopkins]

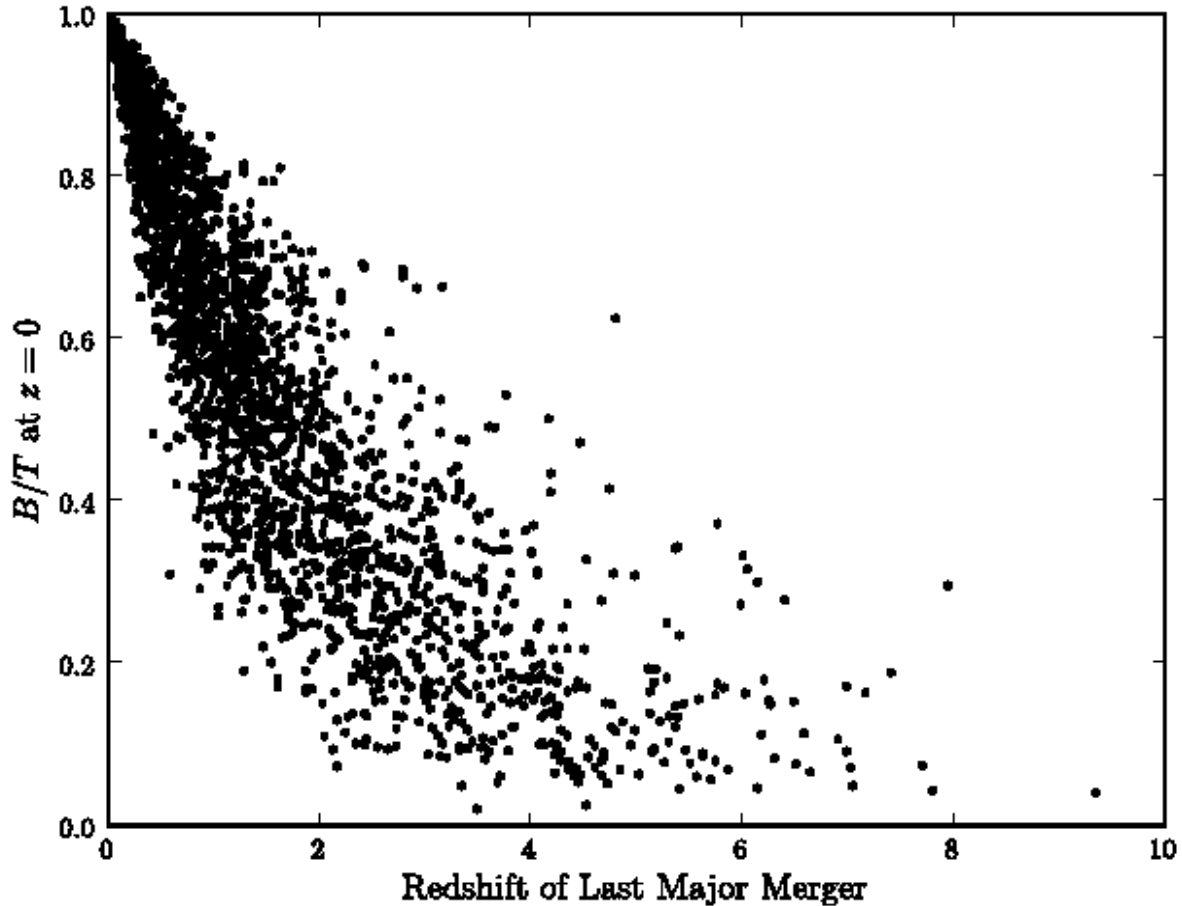


Fig. 21.— Only  $\sim 20\%$  of the galaxies in the theoretical models (see § 5.8) experience *both* major and minor mergers over their lifetime, while  $\sim 80\%$  experience *only* minor mergers. For those galaxies that experienced a major merger, the  $B/T$  of the remnant at  $z \sim 0$  is plotted against the redshift  $z_{\text{last}}$  of the last major merger. Systems where the last major merger occurred at earlier times have had more time to grow a disk and thus have a lower  $B/T$  at  $z \sim 0$ . The dispersion in the present-day  $B/T$  at a given  $z_{\text{last}}$  is due to the different times spent by a galaxy in terms of being a satellite versus a central galaxy in a DM halo, since the cooling of gas and the growth of a disk is stopped when a galaxy becomes a satellite. The models imply that *a galaxy with a past major merger can have  $B/T \leq 0.2$  only if its last major merger occurred at  $z > 2$  (lookback times  $> 10$  Gyr)*. The fraction of model galaxies with  $B/T \leq 0.2$  and a past major merger is only  $3.09\% \pm 0.20\%$  (Table 9).

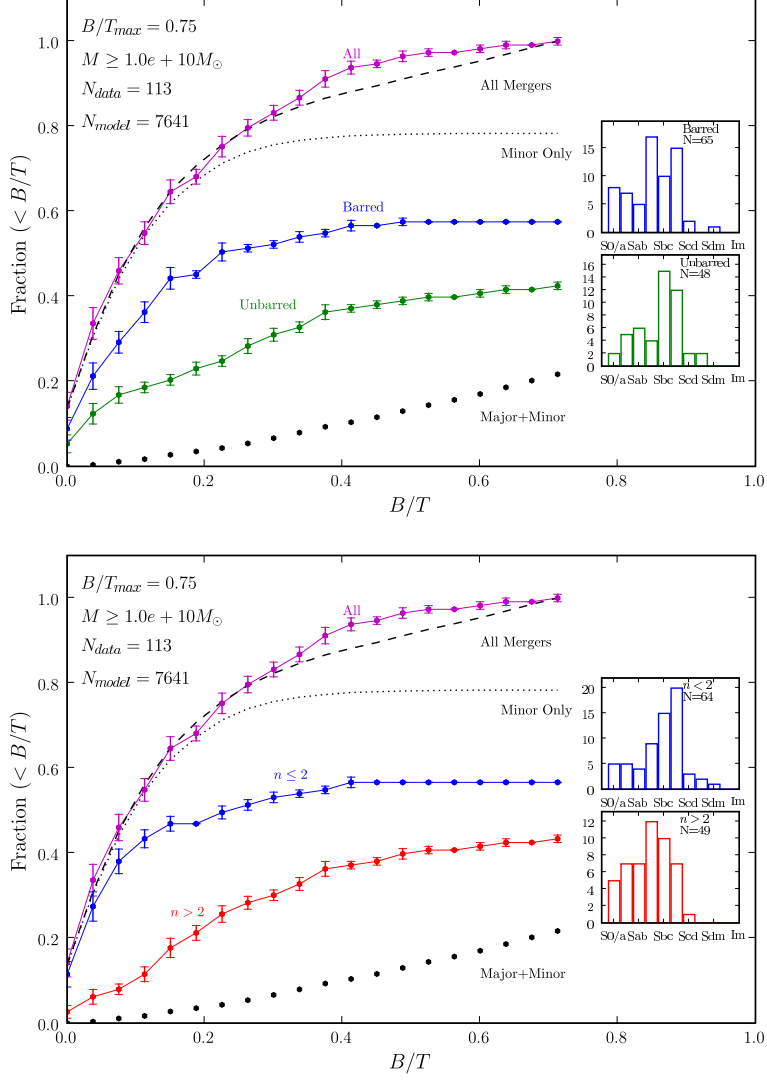


Fig. 22.— The *cumulative* fraction  $F$  of high mass ( $M_\star \geq 1.0 \times 10^{10} M_\odot$ ) spirals with  $B/T \leq$  the x-axis value is shown for the data (colored lines/ points) and for the theoretical model (black lines/points) described in § 5.8. Model and data spirals are defined as systems with  $B/T \leq 0.75$ . The magenta line shows  $F$  from the data, while the other two colored lines break this  $F$  in terms of bar class (top panel) or bulge  $n$  (lower panel). The black dashed line shows  $F$  from all model galaxies, while the black dotted line and black dots show the contribution of model galaxies that experienced, respectively, *only past minor mergers* and *both major and minor mergers*. Major mergers are defined here as those with  $M_1/M_2 \geq 1/4$ . In the models, the fraction ( $\sim 3\%$ ) of high mass spirals, which have undergone a past major merger and host a bulge with  $B/T \leq 0.2$  is a factor of over 15 smaller than the observed fraction ( $\sim 66\%$ ) of high mass spirals with  $B/T \leq 0.2$ . Thus, *bulges built via major mergers seriously fail to account for most of the low  $B/T \leq 0.2$  bulges present in  $\sim 66\%$  high mass spirals*. The majority of such bulges exist in systems that have experienced *only minor mergers, but no major mergers*. They can be built via minor mergers and secular processes. In this realization of the models, where only bulge-building via minor mergers is implemented, the bulges built via minor mergers can account for most of the  $B/T \leq 0.2$  bulges (Table 9).

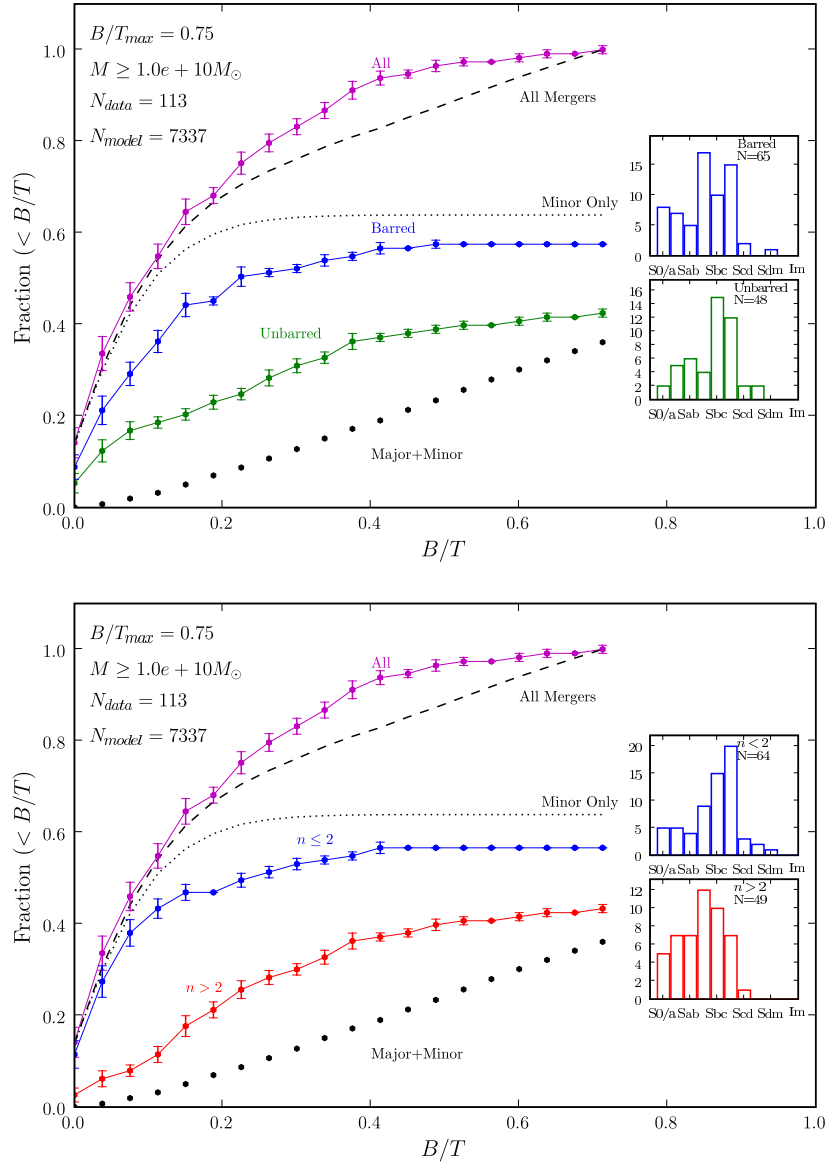


Fig. 23.— This figure is similar to Fig. 22, except that the model now defines major mergers as those with mass ratio  $M_1/M_2 \geq 1/6$ . In this case, about 30% of the model spirals undergo major mergers over their lifetime rather than  $\sim 20\%$ . The overall model  $F$  (black dashed line) now underpredicts the data  $F$  by about 10% for  $B/T > 0.2$ . However, the main conclusion that bulges built by major mergers cannot account for most of the low  $B/T \leq 0.2$  bulges, present in a large percentage ( $\sim 66\%$ ) of spirals still holds.

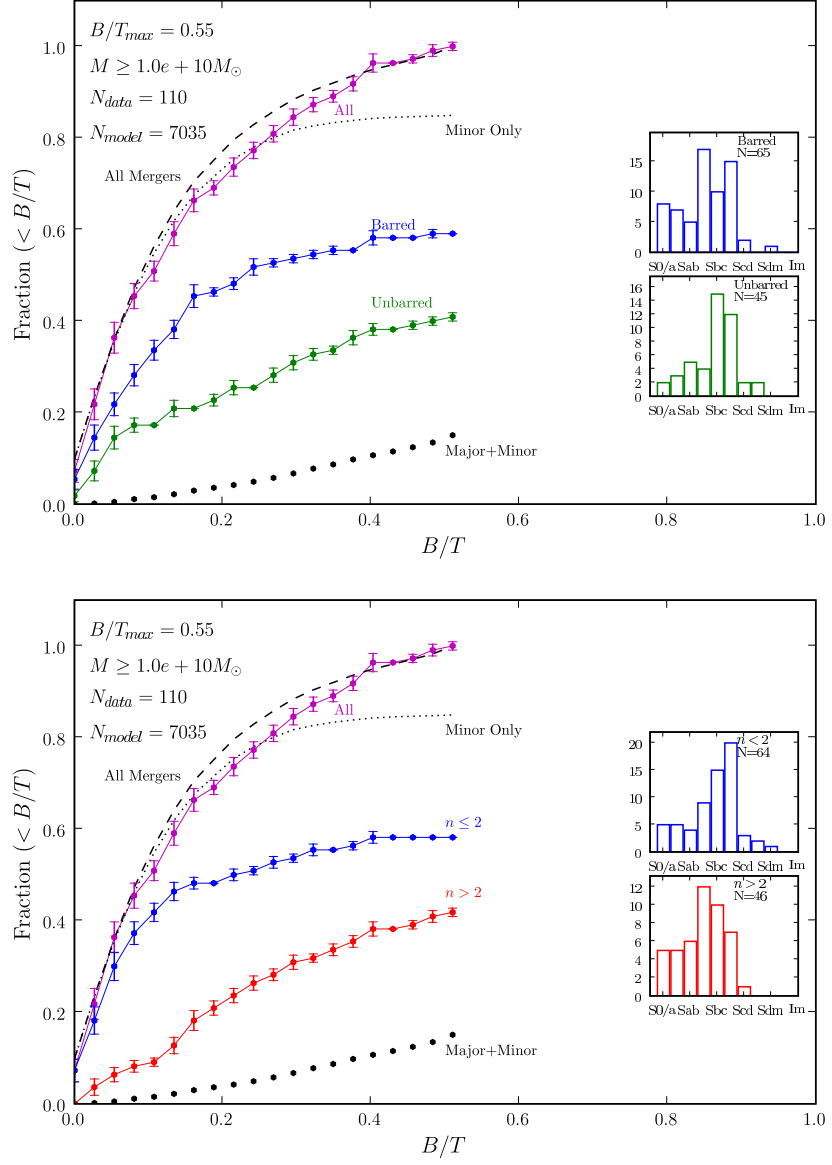


Fig. 24.— This figure is similar to Fig. 22, except that here spirals are considered to be systems with a  $B/T \leq 0.55$  rather than 0.75 in the models, and a corresponding cut is applied to the data points. The results are similar to Fig. 22.

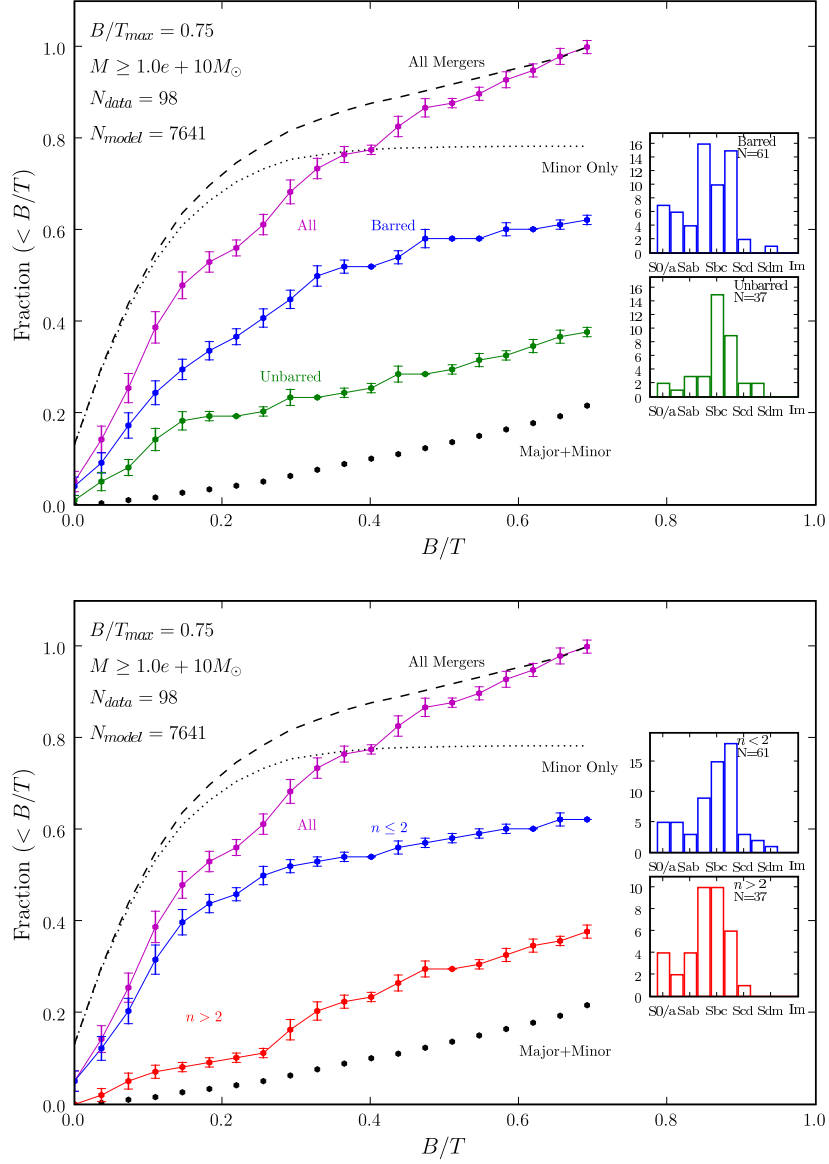


Fig. 25.— This figure is similar to Fig. 22, except that  $B/T$  of all the observed galaxies has been multiplied by a factor of two, in order to test what would happen in the case where the  $M/L$  ratio of the bulge in  $H$ -band is twice as high as that of the disk and bar. This could happen in an extreme example where the dominant bulge stellar population was much older (e.g. 12 Gyr) than the age of the dominant disk stellar population (e.g., 3 Gyr). In such a case the fraction of high mass spirals with  $B/T \leq 0.2$  would change from  $\sim 66\%$  in Fig. 22 to  $\sim 55\%$ , and deviate from the model overall model  $F$  (black dashed line) by  $\sim 20\%$ . However, the main conclusion that bulges built by major mergers cannot account for most of the low  $B/T \leq 0.2$  bulges, present in a large percentage ( $\sim 55\%$ ) of spirals still holds.